Himalayan gneiss dome formation in the middle crust and exhumation by normal faulting: New geochronology of Gianbul dome, northwestern India

Forrest Horton[1,†], Jeffrey Lee[2], Bradley Hacker[1], Meilani Bowman-Kamaha'o[2], and Michael Cosca[3]
[1]*Department of Earth Science, University of California, Santa Barbara, California 93106, USA*
[2]*Department of Geological Sciences, Central Washington University, Ellensburg, Washington 98926, USA*
[3]*U.S. Geological Survey, Denver, Colorado 80225, USA*

ABSTRACT

A general lack of consensus about the origin of Himalayan gneiss domes hinders accurate thermomechanical modeling of the orogen. To test whether doming resulted from tectonic contraction (e.g., thrust duplex formation, antiformal bending above a thrust ramp, etc.), channel flow, or via the buoyant rise of anatectic melts, this study investigates the depth and timing of doming processes for Gianbul dome in the western Himalaya. The dome is composed of Greater Himalayan Sequence migmatite, Paleozoic orthogneiss, and metasedimentary rock cut by multiple generations of leucogranite dikes. These rocks record a major penetrative D2 deformational event characterized by a domed foliation and associated NE-SW–trending stretching lineation, and they are flanked by the top-down-to-the-SW (normal-sense) Khanjar shear zone and the top-down-to-the-NE (normal sense) Zanskar shear zone (the western equivalent of the South Tibetan detachment system). Monazite U/Th-Pb geochronology records (1) Paleozoic emplacement of the Kade orthogneiss and associated granite dikes; (2) prograde Barrovian metamorphism from 37 to 33 Ma; (3) doming driven by upper-crustal extension and positive buoyancy of decompression melts between 26 and 22 Ma; and (4) the injection of anatectic melts into the upper levels of the dome—neutralizing the effects of melt buoyancy and potentially adding strength to the host rock—by ca. 22.6 Ma on the southwestern flank and ca. 21 Ma on the northeastern flank. As shown by a northeastward decrease in $^{40}Ar/^{39}Ar$ muscovite dates from 22.4 to 20.2 Ma, ductile normal-sense displacement within the Zanskar shear zone ended by ca. 22 Ma, after which the Gianbul dome was exhumed as part of a rigid footwall block below the brittle Zanskar normal fault, tilting an estimated 5°–10°SW into its present orientation.

INTRODUCTION

In the predominantly contractional India-Asia collision zone, Himalayan gneiss domes are prevalent—yet seemingly paradoxical—extensional structures that have been attributed to a surprising number of different processes. Three mechanisms were proposed by early researchers to explain the North Himalayan gneiss domes in the eastern portion of the orogen: (1) thrust duplex formation as a result of north-south contractional folding (Burg et al., 1984; Hauck et al., 1998; Makovsky et al., 1999), (2) diapiric rise of anatectic melts (Le Fort, 1986; Le Fort et al., 1987), and (3) Cordilleran-style metamorphic core complex formation (Chen et al., 1990). Subsequent research has highlighted the complexity of Himalayan gneiss dome formation and led to doming models that involve feedback among multiple mechanisms. For example, dome formation has been explained by shear heating–induced melting and diapirism (Harrison et al., 1997), antiformal doming within the hanging wall of a thrust fault superseding diapirism (Lee et al., 2004), and granitic magmas advecting heat that causes extension and anatexis (Aoya et al., 2005).

Himalayan gneiss domes have also been interpreted in the context of the middle-crust channel-flow model (e.g., Nelson et al., 1996; Beaumont et al., 2001; Grujic et al., 2002; Langille et al., 2010), which predicts partial melting and foreland-directed extrusion of Indian crust sandwiched between the South Tibetan detachment system above and the Main Central thrust below. Exhumation of the Greater Himalayan Sequence of gneisses and anatectic leucogranites between these structures can be explained by low viscosity in the middle crust, a horizontal gravitational potential energy gradient, and high denudation rates along the range front (Beaumont et al., 2001, 2004). In this context, plugging of the midcrustal channel due to inefficient surface denudation—coupled with localized extension in overthickened upper crust—could favor exhumation of middle crust in hinterland domes rather than in a channel (Beaumont et al., 2004; Jamieson et al., 2006). The parallel tectonic histories for the Greater Himalayan Sequence and the North Himalayan gneiss domes imply that southward flow of ductile middle crust and doming were coeval and related processes (Lee et al., 2006). Whereas the majority of Himalaya gneiss domes are associated with north-south extension, a subset of younger (and possibly unrelated) domes formed during orogen-parallel extension (e.g., Hintersberger et al., 2010).

Unlike the eastern part of the Himalayan orogen, where gneiss domes form a distinct belt north of the E-W–striking South Tibetan detachment system (Le Fort, 1986), gneiss domes in the western Himalaya are exposed south of and in the footwall of the western continuation of the South Tibetan detachment system (Herren, 1987; Kündig, 1989). Noting that the westernmost gneiss domes commonly have Paleozoic orthogneiss cores, Kündig (1989) proposed that lithologic heterogeneities contributed to preferential exhumation of low-density orthogneiss relative to the surrounding metasedimentary rocks, and that heat transfer by granites caused localized anatexis along their margins. Dèzes et al. (1999), however, attributed regional doming to late-stage isostatic uplift in the footwall of a low-angle normal fault (analogous to Cordilleran-style metamorphic core complex formation). Recent interpretations of Gianbul dome reflect polarized views of northwestern Himalayan tectonic evolution: Gianbul dome is either framed in the context of (1) a thermo-mechanical channel-flow model (Beaumont et al., 2004; Searle et al., 2007), or (2) a structural tectonic wedge model

†E-mail: forrest.horton@gmail.com.

 doi: 10.1130/B31005.1; 10 figures; 2 tables; Data Repository item 2014258.

(Yin, 2006; Webb et al., 2007, 2013), in which the Greater Himalayan Sequence thrust wedge propagates southward below the alternating motion of a roof fault. Based on channel-flow models, Robyr et al. (2002) proposed that inefficient surface denudation and a weak upper crust caused doming. Elaborating upon this hypothesis, Robyr et al. (2006) suggested that the overlying metasedimentary rocks acted as a backstop for the ductile exhumation of the Greater Himalayan Sequence gneisses and migmatites and that decompression led to a positive feedback with partial melting and enhanced exhumation. In the tectonic wedge model, however, Gianbul dome represents the southeastern extent of a regional Greater Himalayan Sequence antiform that inherited irregular topography of the thrust ramp or underwent bending during underthrusting (Yin, 2006).

To address the lack of consensus about gneiss domes in general, and to reevaluate doming mechanisms in the western Himalaya, we present new structural observations, monazite U/Th-Pb geochronology, and $^{40}Ar/^{39}Ar$ mica thermochronology for Gianbul dome. Our data suggest that doming (1) occurred in the middle crust during upper-crustal extension, (2) was driven by positive feedback between decompression melting of metasedimentary rocks and buoyancy-driven exhumation, and (3) ceased prior to brittle exhumation in the footwall of a normal fault. These results have implications for the tectonic evolution of the Himalaya and improve our understanding of gneiss dome formation in continental collision zones worldwide.

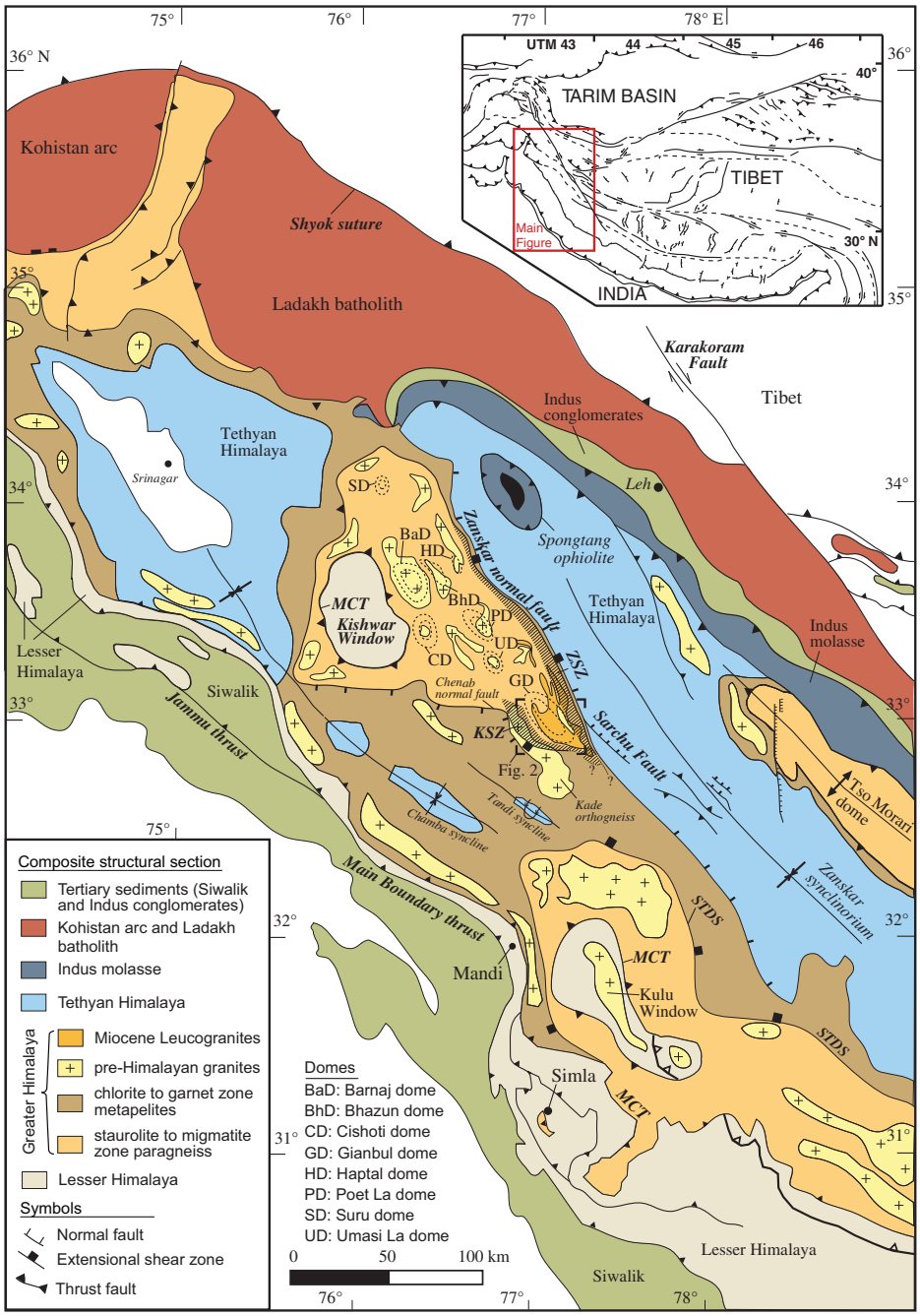

Figure 1. Regional geology map the northwestern Himalaya, modified from Thakur (1998) and Yin (2006). Gianbul dome is exposed in the footwall of Zanskar normal fault, which separates low-grade Tethyan sediments from underlying Greater Himalayan metamorphic rocks. MCT—Main Central thrust; ZSZ—Zanskar shear zone; KSZ—Khanjar shear zone; STDS—South Tibetan detachment system.

GEOLOGIC BACKGROUND

Regional Setting

In the western Himalaya, high-grade metamorphic rocks from the middle crust are exposed as the Greater Himalayan Sequence (also referred to as the High Himalayan Crystalline Sequence), bounded by the northeast-dipping Main Central thrust to the southwest, and separated from overlying Tethyan Himalayan sediments by the 150-km-long Zanskar shear zone, the western extent of the South Tibetan detachment system, to the northeast (Fig. 1). In the Zanskar region of northwest India, the Greater Himalayan Sequence consists of Precambrian fine-grained biotite paragneisses and Precambrian–Early Cambrian Phe metapelites (Herren, 1987), Cambrian–Ordovician K-feldspar augen gneiss (Frank et al., 1977; Mehta, 1977; Stutz and Thöni, 1987; Pognante et al., 1990; Noble and Searle, 1995; Walker et al., 1999; this study), and several Mississippian–Permian orthogneiss bodies (Honegger et al., 1982; Spring et al., 1993; Noble et al., 2001; Horton and Leech, 2013). Peak Barrovian, M1, metamorphism related to crustal thickening reached 550–680 °C and 0.8–1.0 GPa (Dèzes et al., 1999; Searle et al., 1999; Walker et al., 2001; Robyr et al., 2002) at ca. 35–30 Ma (Vance and Harris, 1999; Walker et al., 1999); the M1 metamorphic isograds (chlorite to kyanite) define domes (Herren, 1987; Kündig, 1989; Stäubli, 1989). The isograds are telescoped in the footwall of the Zanskar shear zone (Herren, 1987; Searle and Rex, 1989; Dèzes et al., 1999; Walker et al., 2001; Robyr et al., 2002) and overprinted by a sillimanite-

grade, M2, metamorphism and anatexis at 650–770 °C and 0.45–0.7 GPa (Searle et al., 1999; Robyr et al., 2002). Cenozoic migmatites, leucogranite dikes, and small plutons are prevalent (Honegger et al., 1982; Searle and Fryer, 1986; Noble and Searle, 1995), especially near Paleozoic orthogneisses (Kündig, 1989).

Gianbul Dome Geology

Gianbul dome is bounded by the NE-dipping Zanskar shear zone in Gianbul Valley and the SW-dipping Khanjar shear zone in Miyar Valley (Figs. 2 and 3). The core of Gianbul dome is composed of migmatitic paragneiss (Fig. 4A) mantled by metasedimentary rocks (Fig. 4B) and orthogneiss (Fig. 4C), which are cut by multiple generations of leucogranite dikes (Fig. 4D; Dèzes et al., 1999; Robyr et al., 2002, 2006, 2014; this study). The Precambrian to Cambrian Phe paragneiss includes aluminosilicates + garnet + biotite + muscovite. The Paleozoic Kade orthogneiss in the Miyar Valley contains metamorphic garnet and foliated biotite-rich melanosomes that indicate local migmatization (Pognante et al., 1990; Dèzes, 1999). Textures demonstrate that Cenozoic leucogranites and pegmatites were derived from the migmatites: leucogranites intermingle with leucosomes in the core of the dome, cut gneisses as a stockwork of dikes, and form sill-like bodies concordant to the gneissic foliation.

Migmatites, metasedimentary rocks, and orthogneiss record two primary Cenozoic ductile deformation events (earlier pre-Himalayan deformation is manifested elsewhere by Cambrian–Ordovician granites that cut structures in metasedimentary rocks; Gehrels et al., 2003). The oldest Cenozoic deformation, D1, is characterized by contractional structures related to NE-SW shortening and vertical thickening. Regional contraction produced the largely brittle nappe system in the Tethyan Himalayan sequence north of Gianbul dome, and the underlying ductile "Crystalline" or "Shikar Beh" nappe that makes up the Greater Himalayan Sequence (Steck et al., 1993; Epard and Steck, 2004). Extensional deformation, D2, that largely overprints D1 is associated with orogen-scale extensional slip along the Zanskar shear zone and doming (Dèzes et al., 1999; Robyr et al., 2002).

Ductile deformation within Gianbul dome is concentrated within two prominent shear zones: (1) the ~15-km-wide Zanskar shear zone on the northeastern flank of the dome and (2) the ~16-km-wide Khanjar shear zone on the southwestern flank (Fig. 2B). Both shear zones have complex multistage deformation histories. In the Zanskar shear zone, syntectonic garnets and sigma clasts are thought to represent D1 top-to-the-SW thrusting along the boundary between the Tethyan and crystalline nappe systems (Dèzes et al., 1999). In the Khanjar shear zone, top-to-the-NE syntectonic garnets, C-S fabrics, and sigmoidal K-feldspar clasts (e.g., Fig. 4E) have also been attributed to D1 thrusting (Robyr et al., 2002, 2014), but some or all of these fabrics could alternatively represent early D2 extension later transposed during doming. If contractional features on both limbs are relics of D1 burial, it remains unclear whether the opposing D1 contractional shear zones were parallel prior to doming or intersected in the now-eroded upper levels of the dome. Extensional D2 deformation is better understood: Both shear zones clearly exhibit a well-developed, high-strain S2 foliation that dips moderately to the NE within the Zanskar shear zone and moderately to the SW in the Khanjar shear zone and is associated with a NE-trending stretching lineation (Figs. 2B and 4F). As noted by Robyr et al. (2006), the absence of a thrust structure between the Zanskar shear zone and the Khanjar shear zone suggests coeval extension along both shear zones.

Mesoscopic and microscopic structures within both shear zones, including asymmetric boudins of leucocratic dikes and quartz veins, shear bands, S-C fabrics, asymmetric tails on K-feldspar porphyroclasts, asymmetric grain shape foliations, and asymmetric crystallographic preferred orientations (CPOs) of quartz, record the senses of shear associated with the development of the S2 foliation (Figs. 5 and 6; Dèzes et al., 1999; Robyr et al., 2006; this study). Kinematic structures exposed across the Khanjar shear zone are dominated by top-down-to-the-SW senses of shear (Figs. 2B, 5A, 5B, and 6), but top-up-to-the-NE shear indicators are exposed locally (Figs. 4E and 5C). Kinematic fabrics exposed across the Zanskar shear zone in Gianbul Valley are almost exclusively characterized by top-down-to-the-NE senses of shear (Figs. 2B, 5D, 5E, and 6).

There has been considerable debate as to whether the Zanskar shear zone and Khanjar shear zone are part of the same detachment fault system. Thakur (1998) and Dèzes et al. (1999) inferred that the Zanskar shear zone bends southward around Gianbul dome and joins the Khanjar shear zone and Chenab normal fault. This view suggests that the entire Greater Himalayan Sequence exposure in the northwestern Himalaya forms an antiformal window surrounded by normal faults (Thakur, 1998; Yin, 2006). Because no equivalent of the Zanskar shear zone–Khanjar shear zone fault exists south of Gianbul dome and the Chenab normal fault, Yin (2006) postulated that the Zanskar shear zone and Main Central thrust merge at depth. The counterview, that the Khanjar shear zone and Zanskar shear zone are discrete structures, is based on two lines of reasoning. First, syntectonic garnets in the Khanjar shear zone suggest that top-to-the-NE shearing occurred during burial and, therefore, before top-to-the-NE extensional shearing in the Zanskar shear zone (Robyr et al., 2002, 2014). Second, mapping by Epard and Steck (2004) showed that the Zanskar shear zone bends southward around Gianbul dome—but not entirely—and can be followed eastward into a series of low-angle brittle normal faults that presumably connect with eastern segments of the South Tibetan detachment system. These early extensional faults are cut by steeper brittle faults (Epard and Steck, 2004) associated with the NE-dipping Zanskar normal fault that caps the Zanskar shear zone (Inger, 1998). Steep conjugate normal faults also cut the Zanskar shear zone hanging wall and splay into the Tethyan metasedimentary rocks (Dèzes et al., 1999; Searle et al., 2007). No equivalent brittle extensional structures have been observed above the Khanjar shear zone.

Minimum displacement along the Zanskar shear zone, based on the distance between metamorphic isograds (Herren, 1987), telescoped thermobarometric estimates of peak pressure in the garnet and kyanite zones (Dèzes et al., 1999), telescoped deformation temperatures (Stahr, 2013), and orientation of sheared dikes (Finch et al., 2014), is estimated at between 15 and 40 km. Considering that quartz microstructures in the Zanskar shear zone record a pure-shear component of deformation (Hasalova and Weinberg, 2011), this may be an overestimate of ductile displacement because of the assumption of 100% simple shear in these calculations. Also, a significant fraction of the net slip—60 km is required to exhume the migmatite core from >30 km depth at a dip of 20°—may have occurred during late-stage brittle faulting. If the Zanskar shear zone originally had a gentler dip (<10° for example), the offset could have been >100 km (Dèzes, 1999); similarly high estimates of net slip have been proposed for the South Tibetan detachment in the eastern Himalaya based on mineral assemblage pressure estimates (Searle et al., 2003), telescoped isotherms (Law et al., 2011), and INDEPTH seismic-reflection profiles and the restoration of Tethyan sedimentary sequences (Hauck et al., 1998). Displacement along the Zanskar shear zone in Gianbul dome should be viewed as a maximum for the western Himalaya because the apparent total shear along the Zanskar shear zone decreases to the NW (Inger, 1998). Beyond the eastern terminus of the ductile Zanskar shear zone, poor exposure precludes estimations of total offset along brittle normal faults (Epard and Steck,

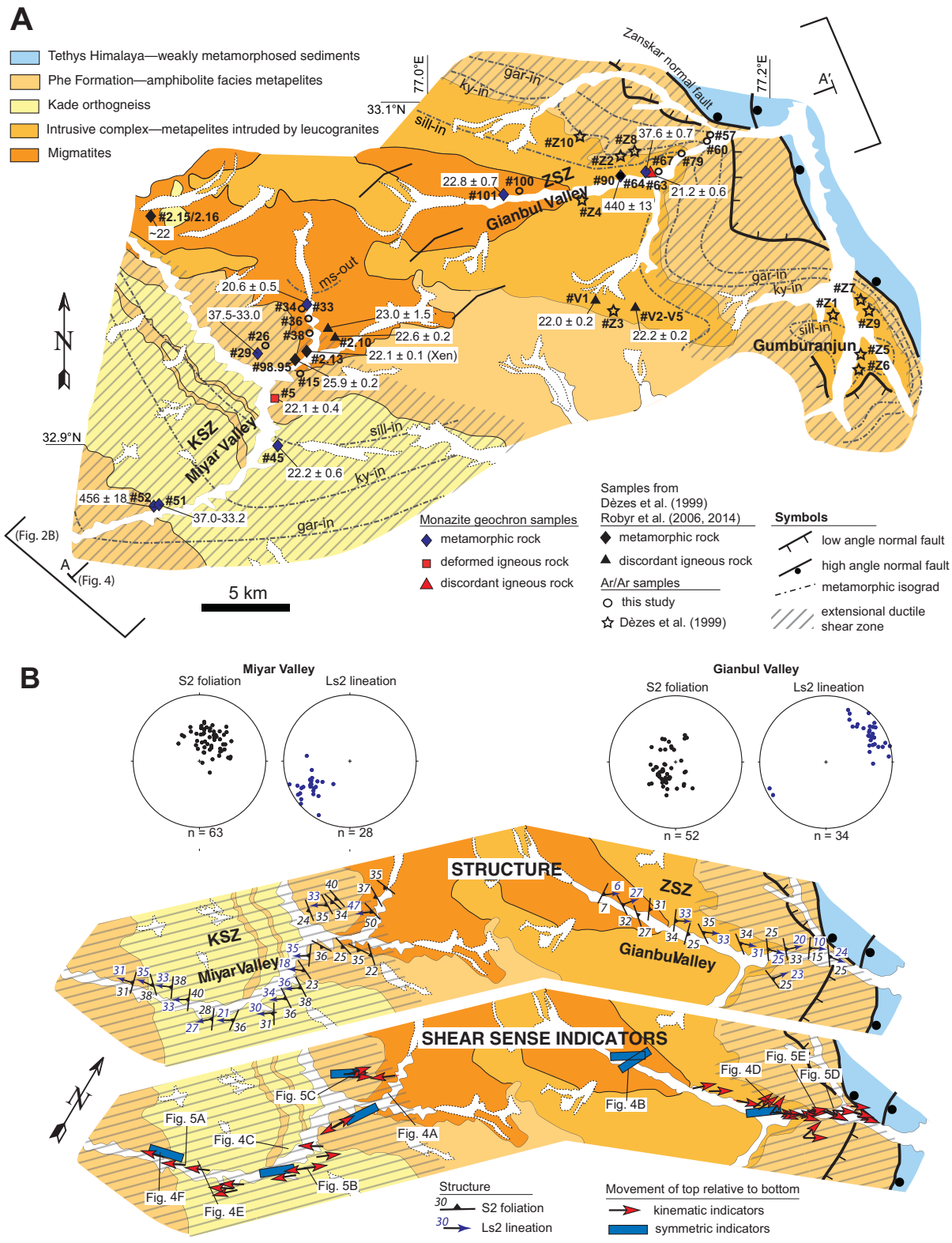

Figure 2. (A) Geologic map of the Gianbul study area (from Dèzes, 1999; Robyr et al., 2006, 2014; this study) showing major lithologic units, Barrovian metamorphic isograds, shear zones, and sample locations. Monazite U/Th-Pb ages from this study (color) and literature (black) are reported in Ma (Xen—xenotime, gar—garnet, sill—sillimanite, ky—kyanite, ms—muscovite). ZSZ—Zanskar shear zone; KSZ—Khanjar shear zone. (B) Structural data and kinematic shear-sense indicators along a NE-SW transect of Gianbul dome, as well as lower-hemisphere projection stereonets for S2 foliation and Ls2 lineation measurements.

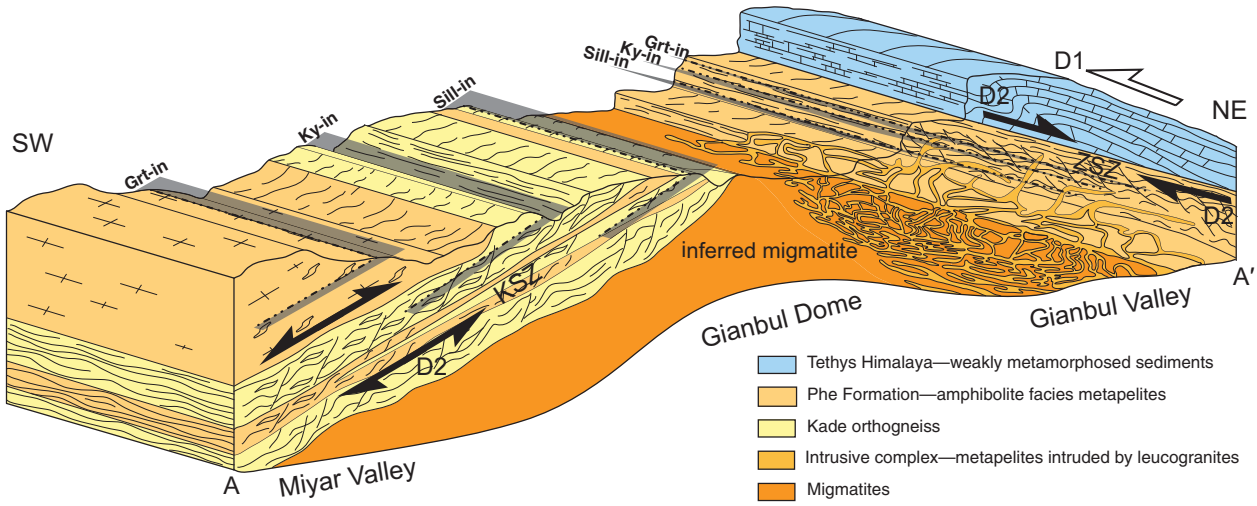

Figure 3. Generalized synthetic block diagram for Gianbul dome along the Miyar Valley–Gianbul Valley transect (modified from Robyr et al., 2006; Grt—garnet, Sill—sillimanite, Ky—kyanite). Migmatite, metasediment, and orthogneiss record two ductile deformation events: D1 contractional related to NE-SW shortening and vertical thickening and D2 ductile NE-SW extension that overprints D1 structures. The Zanskar shear zone (ZSZ) and Khanjar shear zone (KSZ) were most likely segments of the same planar top-to-the-NE extensional shear zone before doming transposed the Khanjar shear zone into its present-day orientation (see text for explanation). Leucogranites from migmatite zones in the Gianbul Valley intruded metasediments during late D2 deformation and after doming ended.

2004), making it difficult to estimate the tectonic significance of these structures.

The grade of M1 Barrovian metamorphism increases from garnet zone on the flanks of Gianbul dome to migmatites in the core. Textural evidence indicates that this metamorphism occurred during D1, and thermobarometry suggests peak conditions of ~800 °C and 1.2 GPa (Pognante and Lombardo, 1989; Dèzes et al., 1999; Robyr et al., 2002). Near-isothermal decompression led to a second metamorphism, M2, which was synchronous with the D2 extension and characterized by growth of fibrolite, garnet, cordierite, and retrograde andalusite (Dèzes et al., 1999; Robyr et al., 2002; this study). The stability of biotite during both metamorphic events suggests that muscovite breakdown was principally responsible for melt generation, which constrains peak temperatures to <850 °C (Dèzes et al., 1999). Temperatures were probably highest in the core of the dome, but thermometry based on Fe-Mg exchange and oxygen isotopes uniformly indicates ~800 °C across melted and unmelted metasedimentary units (Robyr et al., 2002).

GEOCHRONOLOGY AND THERMOCHRONOLOGY

U/Th-Pb Geochronology Results

To constrain the timing of ductile deformation, in situ laser-ablation split-stream (LASS) inductively coupled plasma–mass spectrometry (ICP-MS) U/Th-Pb monazite geochronology and trace-element geochemistry analyses were conducted on monazites and zircons in 10 metamorphic and igneous thin sections. (Table 1; see Table DR1 for analytical data, DR2 for LASS methods, and DR3 for petrologic sample descriptions[1]). Samples were collected along a NE-SW transect across Gianbul dome, subparallel to the D2 stretching lineation (Fig. 2). Metamorphic samples were analyzed to place temporal constraints on the pressure-temperature (*P-T*) evolution of the dome; orthogneisses proved most useful because they (1) are the dominant lithology in Miyar Valley, (2) contain abundant monazite, and (3) preserve both D1 contraction and D2 extension. Several samples, however, yielded igneous protolith dates rather Cenozoic metamorphic dates. Deformed and nondeformed Miocene granites were analyzed to constrain the late stages and termination of ductile extension.

Paleozoic Dates

Most of the metamorphic rocks analyzed have Cenozoic monazite dates, but two samples preserve Paleozoic igneous protolith crystallization dates. Sample 52b is from the top of the main megacrystic Kade orthogneiss body in Miyar Valley that intrudes overlying Phe metasediments within the garnet zone. At this outcrop, top-to-the-NE shear fabrics are overprinted by dominant D2 top-to-the-SW shear fabrics (Fig. 5A). Textures common to all orthogneiss samples—equant to elongate quartz grains with equant subgrains and bent, twinned, and cracked feldspar—are compatible with strong deformation at amphibolite-facies conditions. Monazites in sample 52b occur primarily in porphyroclastic garnets; some have been partially replaced by allanite, apatite, and zircon. Eleven concordant analyzes of 52b monazites yield an igneous emplacement concordia date of 466 ± 10 Ma (Fig. 7A). To avert potential effects of minor Pb loss, this date was calculated using the maximum number of spot analyses consistent with a single population.

Sample 90b is from an orthogneiss intruding Phe metasediments in the sillimanite zone of Gianbul Valley. This orthogneiss has a well-developed D2 structural fabric, including top-to-the-NE shear indicators, and it is crosscut by multiple generations of stockwork dikes that extend from the migmatites below to the intrusion complex above, where sills are concordant with the host metapelite S2 foliation. Euhedral to subhedral monazite grains in sample 90b have igneous oscillatory zoning textures and surface embayments indicative of partial dissolution. The oldest six analyses have an igneous emplacement concordia date of 471 ± 11 Ma (Fig. 7B). The abundance of monazite in orthogneisses—as well as differing degrees of mona-

[1]GSA Data Repository item 2014258, DR1, analytical data; DR2, LASS methods; DR3, petrologic sample descriptions; DR4, analytical data; DR5, $^{40}Ar/^{39}Ar$ methods; and DR6, biotite $^{40}Ar/^{39}Ar$ age spectra, is available at http://www.geosociety.org/pubs/ft2014.htm or by request to editing@geosociety.org.

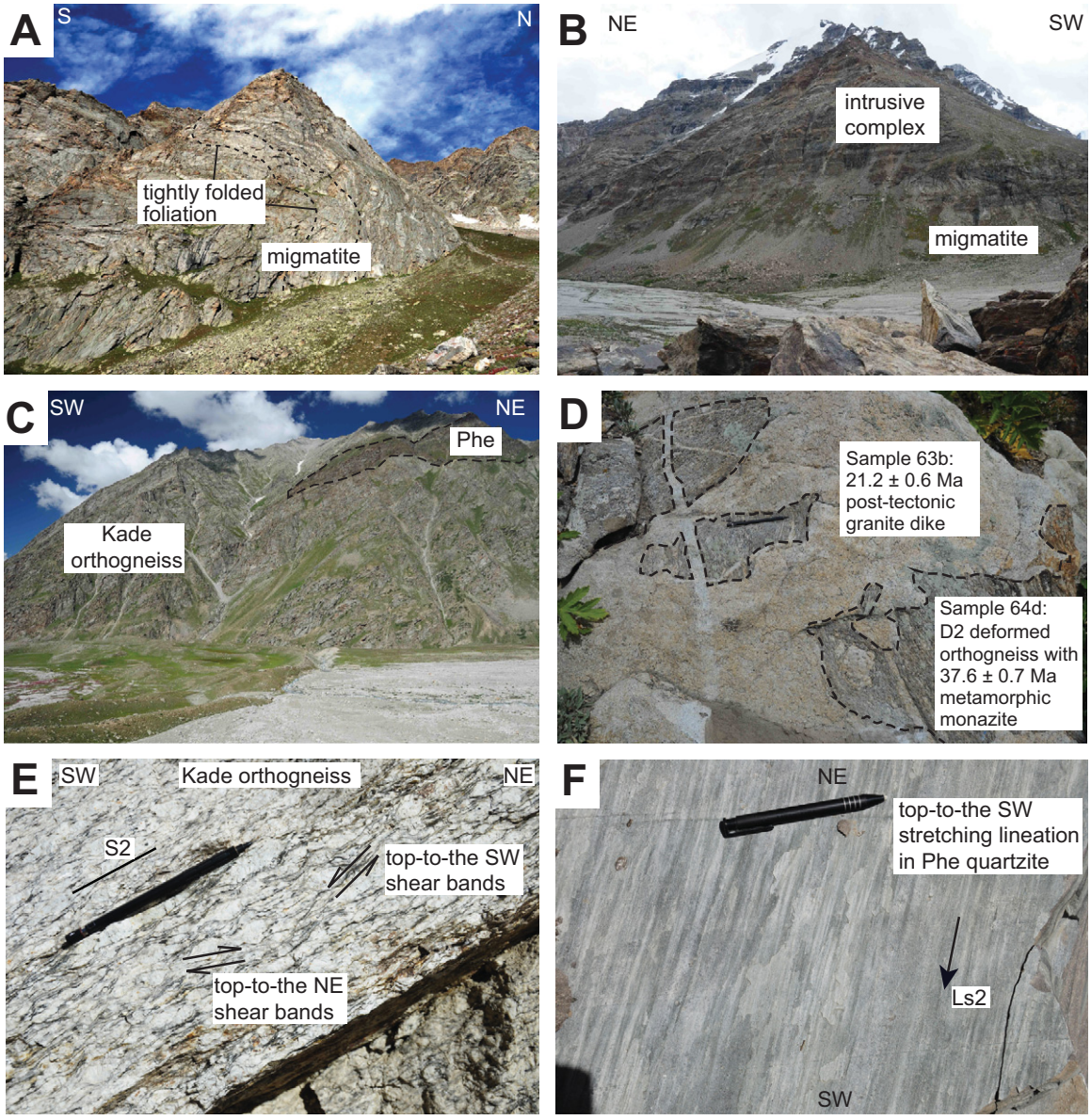

Figure 4. Photographs illustrating mesoscopic and microscopic field relations and textures (see Fig. 2B for locations). (A) Tightly folded migmatite in the core of the dome exposed in Miyar Valley. (B) Intrusive complex overlying migmatite core in Gianbul Valley with well-developed compositional banding (S2 foliation) dipping to the northeast. (C) Kade orthogneiss intruding Phe metapelite in Miyar Valley with well-developed S2 foliation dipping to the southwest. (D) Deformed orthogneiss in Gianbul Valley with K-feldspar megacrysts crosscut by a nondeformed dike. (E) K-feldspar sigma-clasts in Kade orthogneiss showing top-to-the-NE and top-to-the-SW shear bands. Outcrop face is approximately perpendicular to the S2 foliation and parallel to the Ls2 stretching lineation. (F) Top-to-the-SW stretching lineations in Phe quartzite in Miyar Valley.

zite dissolution/precipitation during Cenozoic orogenesis—seems independent of metamorphic grade, suggesting that a range in bulk composition may account for the variability.

Cenozoic Metamorphic Dates

Eocene to early Oligocene metamorphic dates that span Gianbul dome are broadly attributed to D1 burial-related deformation and M1 prograde metamorphism. Sample 64d is from a minor megacrystic orthogneiss body in the upper portion of the intrusive complex in Gianbul Valley, amid sillimanite zone Phe metapelites and leucogranite sills. Sigma-shaped K-feldspar clasts preserve top-to-the-NE shear fabrics and are cut by nondeformed post-tectonic leucogranite dikes (Fig. 4D). Subhedral monazites are found in a quartz and feldspar matrix and have Y-rich cores with subtle oscillatory zoning, as well as embayments indicative of partial dissolution. Analyses of sample 64d form a single population of $^{232}Th/^{208}Pb$ dates at 37.6 ± 0.7 Ma (Fig. 7C).

On the far side of the dome, orthogneiss sample 51b from Miyar Valley was collected from the uppermost Kade orthogneiss near overlying Phe metasediments. Sample 51b is in the garnet zone and exhibits discrete greenschist-facies

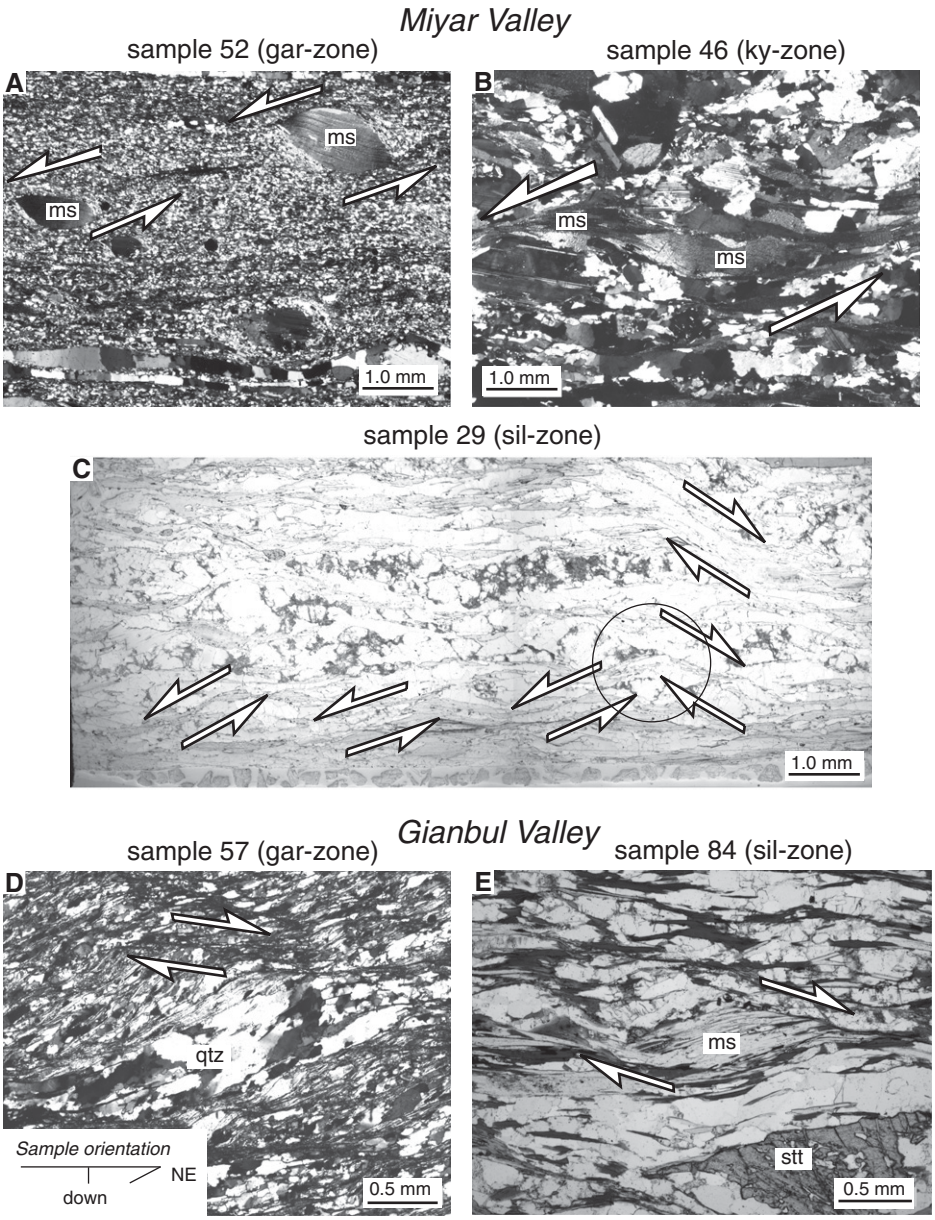

Figure 5. Photomicrographs of shear sense indicators. (A) Mica fish in Kade orthogneiss indicating top-to-the-SW sense of shear. (B) C′-type shear bands in Kade orthogneiss indicating top-to-the-SW sense of shear. (C) C′-type shear bands in Kade orthogneiss indicating both top-to-the-SW and top-to-the-NE senses of shear. Circle shows where, in this photomicrograph, top-to-the-NE C′-type shear band crosscuts top-to-the-SW C′-type shear band. (D) Oblique quartz grain shear foliation and shear bands indicating top-to-the-NE sense of shear. (E) C′-type shear bands indicating top-to-the-NE sense of shear. All photomicrographs are from samples cut parallel to the stretching lineation and perpendicular to the foliation and are cross-polars, except C, which is plane light. Sample orientation shown; arrow pairs indicate sense of shear. Abbreviations: gar—garnet; ky—kyanite; ms—muscovite; qtz—quartz; sil—sillimanite; stt—staurolite.

shear bands. Monazites occur in biotite pressure shadows, and some have been partially replaced by allanite, apatite, and zircon. Subhedral monazites in 51b with compositionally mottled textures have a range of dates from 37.0 to 33.2 Ma (Fig. 7D); a corresponding increase in Th/U may represent a transition from fluid-assisted growth to crystallization in the presence of silicate melt.

Sample 29b is from a tourmaline-bearing orthogneiss dike amid migmatites in the sillimanite zone in Miyar Valley; transposed into the D2 foliation, this dike possesses a well-developed S2 foliation, NE-SW–trending mineral elongation, and both top-to-the-NE and top-to-the-SW kinematic indicators (Fig. 5C). Whereas all other U/Th-Pb analyses were done in situ on thin sections, monazite and zircon mineral separates from sample 29b were mounted and analyzed in an epoxy mount. U-Pb zircon analyses for 29b fall on a mixing line between ca. 485 Ma and ca. 35 Ma (Fig. 7E), recording Paleozoic protolith emplacement and Cenozoic metamorphism that caused rim growth and the annealing of radiation-damaged cores (Fig. 7F). Large (>100 μm) anhedral monazites exhibit oscillatory zoned cores and high-Th/low-Y rims; euhedral core zones have a $^{232}Th/^{208}Pb$ date of 36.7 ± 0.8 Ma, and rims have a date of 33.7 ± 0.7 Ma (Figs. 7F and 7G). Incorporation of ^{230}Th during the growth of the extremely Th-rich rims (~20 wt%) explains excess ^{206}Pb and positive discordance of the younger population. As with sample 51b, Th-rich rims of 29b monazites are attributed to the presence of silicate melt. Unlike sample 51b, however, distinct core and rim zones are suggestive of two distinct crystallization events.

Several metamorphic samples yielded distinctly younger dates. In the kyanite zone of Miyar Valley, sample 45b is from the middle portion of the main Kade orthogneiss body. The orthogneiss has dominant D2 top-to-the-SW shear fabrics overprinting top-to-the-NE shear fabrics. Small (<100 μm) subhedral monazites have patchy compositional variations and are spatially associated with D2 foliation-parallel biotite; these presumably metamorphic monazites have a date of 22.2 ± 0.6 Ma (Fig. 7I). To the northeast, sample 33 is from the migmatite core of the dome in the sillimanite zone of Miyar Valley and has a well-developed S2 gneissic foliation with symmetrical fabrics suggesting bulk pure shear. Sample 33 monazites are elongate and highly anhedral, have patchy compositional zoning, and yield a rather young date of 20.6 ± 0.5 Ma (Figs. 7J and 7K), perhaps related to late-stage fluid-related growth. From the northern core of the dome, sample 101b from the sillimanite zone in Gianbul Valley also possesses S2 gneissic foliation suggestive of bulk pure shear. Sample 101b has microstructures indicative of hypersolidus deformation with little subsequent strain and a well-developed NE-SW–trending mineral stretching lineation, Ls_2. Subhedral 101b monazites that are located mostly in a coarse quartz and feldspar matrix have a date of 22.8 ± 0.7 Ma (Figs. 7L and 7M).

Cenozoic Igneous Dates

Sample 5c is part of a weakly deformed late D2 leucogranite dike swarm in the Miyar Val-

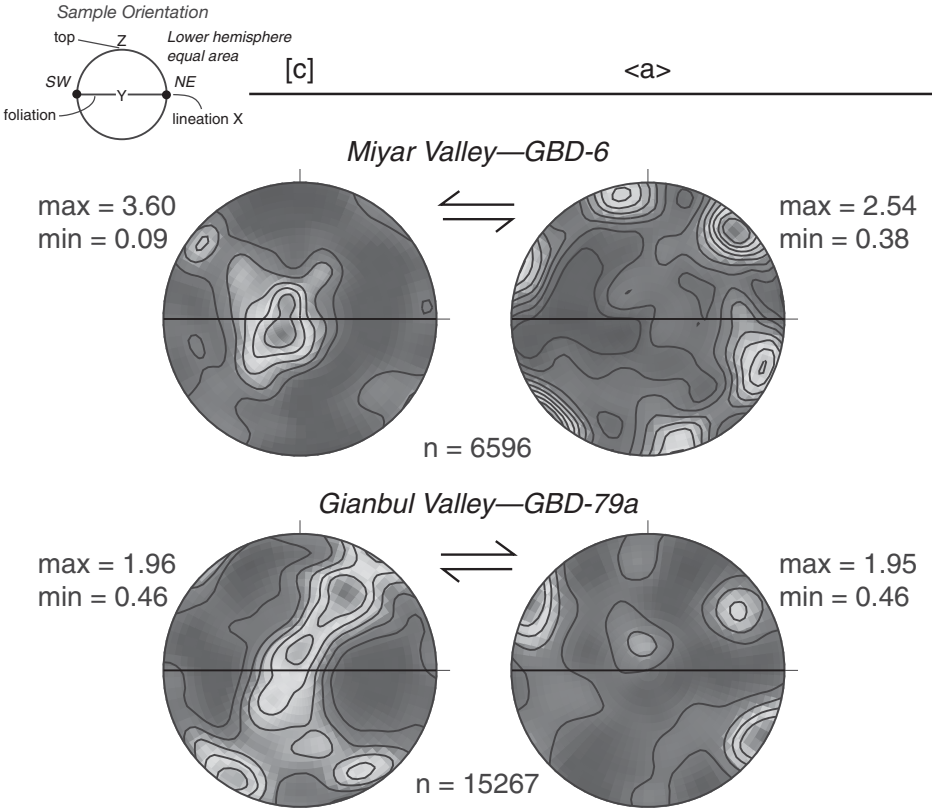

Figure 6. Representative interpretable electron backscatter diffraction (EBSD)–generated quartz crystallographic preferred orientations (CPOs) from sillimanite-zone paragneiss samples from Miyar and Gianbul Valleys cut perpendicular to foliation and parallel to lineation. Lower-hemisphere [c] and <a> axis stereonet plots are shown and oriented as indicated in the sample orientation. Data are point per grain; contours are mean uniform density (m.u.d.) within indicated maximum (max) and minimum (min) values; number (n) of quartz grains were measured as noted. EBSD methods were described by Langille et al. (2010).

ley sillimanite zone that cuts the migmatites, orthogneisses, and metasediments. The S2 foliation feathers a few millimeters into the rims of thick (>1 m) dikes, whereas centimeter-scale dikes are isoclinally folded with an axial plane parallel to the S2 foliation. Small (<100 µm) euhedral monazites in sample 5c have Y-rich cores and an average date of 22.1 ± 0.4 Ma (Fig. 7N), which overlaps with the metamorphic samples. Although cores and rims could not be analyzed separately, the cluster of nearly concordant analyses most likely represents emplacement of the dike prior to the cessation of ductile shearing. Sample 63b is from a nondeformed dike in the upper levels of the intrusion complex in Gianbul Valley that crosscuts metapelites, minor Paleozoic orthogneiss bodies (sample 64d; Fig. 4D), and prior generations of leucogranite dikes. Small (<100 µm) euhedral monazites have Y-rich cores with oscillatory zoning, thin rims, and an average date of 21.2 ± 0.6 Ma (Fig. 7O).

$^{40}Ar/^{39}Ar$ Thermochronology

The $^{40}Ar/^{39}Ar$ thermochronology was conducted on mica separations from rocks across Gianbul dome to evaluate the timing and style of moderate temperature cooling and exhumation (Table 1; see DR4 for analytical data and DR5 for $^{40}Ar/^{39}Ar$ methods [see footnote 1]). Twenty-one samples were analyzed from D2 deformed metapelites, orthogneisses, migmatites, and dikes across the dome along a transect subparallel to the NE-SW–trending Ls_2 stretching lineation (Fig. 2). We report a weighted mean plateau age (WMPA) for those samples in which three or more consecutive steps yield ages within 1σ and comprise more than 50% of the total gas released. In the absence of a WMPA, a preferred age (PA) is reported for consecutive steps that yield a nearly flat spectrum. Errors are reported to 1σ for all ages. The estimated Ar closure temperatures for muscovite are ~415–460 °C (for grain sizes from 100 to 500 µm at cooling rates of ~10 K/m.y. and 0.5 GPa; Kirschner et al., 1996; Harrison et al., 2009), and estimated Ar closure temperatures for biotite are ~320 ± 50 °C (for 150 µm grains at cooling rates of ~10 K/m.y.; Grove and Harrison, 1996).

Sixteen muscovite samples were analyzed from D2 deformed metapelites, orthogneisses, and dikes, and post-tectonic dikes spanning garnet through sillimanite zones. Fourteen of the samples yielded well-defined plateau ages, and two yielded disturbed age spectra (samples 60b and 100b), for which we calculated preferred ages (Fig. 8; Table 1). The age for sample 100b is considered reliable because the analyzed muscovites were mostly inclusion free, whereas sample 60b muscovites contained small inclusions of biotite and, perhaps, tourmaline or graphite. Excluding sample 60b, and accounting for variable sample elevation, muscovite ages for D2 deformed samples decrease northeastward across the dome from 21.4 ± 0.1 Ma in the garnet zone of Miyar Valley to 20.2 ± 0.2 Ma in the garnet zone in Gianbul Valley. The two post-D2 granite dikes from Gianbul Valley yielded ages of ca. 19.8 Ma.

Seventeen biotite samples were analyzed from D2 deformed metapelites, orthogneisses, migmatites, and dikes, and post-tectonic dikes spanning garnet- through sillimanite-zone rocks. Ten of the samples yielded well-defined plateau ages, and seven yielded disturbed age spectra with preferred ages (DR6 [see footnote 1]). Approximately 40% of the biotite ages are older than coexisting muscovite ages regardless of structural depth, suggesting that many of the biotite ages are unreliable. Many biotites contained minor degrees of alteration to chlorite, and some contained muscovite inclusions; they likely incorporated extraneous argon, thus yielding ages older than the coexisting muscovite. The two post-D2 granite dikes from Gianbul Valley yielded biotite ages of ca. 19.7 Ma.

Interpretation of Results

The U/Th-Pb results record three distinct (re) crystallization events: (1) Paleozoic emplacement of the Kade orthogneiss and associated granite dikes, (2) metamorphic monazite crystallization in the presence of melt/fluid (evident from oscillatory zoning) from ca. 37–33 Ma, and (3) metamorphic monazite growth preceding the emplacement of late- to post-tectonic leucogranite dikes from 22 to 21 Ma. These results are broadly consistent with previous geochronology of Gianbul dome by Dèzes et al. (1999) and Robyr et al. (2006, 2014). Metamorphic xenotime from migmatite in the Miyar Valley preserving NE shear sense overprinted by SW-directed shear sense (Robyr sample 2–13) gave

TABLE 1. U/Th-Pb GEOCHRONOLOGY AND ARGON THERMOCHRONOLOGY RESULTS

Sample no.	Latitude (°N)	Longitude (°E)	Lithology		Monazite	±2σ	Zircon	±2σ	Muscovite	±1σ	Biotite	±1σ
Miyar Valley												
GBD-5c	32.93034	76.90175	Pegmatite dike	Deformed	22.1	0.4	N.D.		20.7	0.1	21.3*	0.2
GBD-15	32.94436	76.90836	Pegmatite dike	Deformed	N.D.		N.D.		20.7	0.2	N.D.	
GBD-26c	32.95797	76.88536	Aplite dike	Deformed	N.D.		N.D.		20.7	0.1	21.4	0.2
GBD-29b	32.96137	76.88853	Pegmatite dike	Deformed	36.7–33.7	0.8	485	20	20.7	0.2	N.D.	
GBD-33	32.98282	76.91902	Biotite migmatite	Deformed	20.6	0.5	N.D.		N.D.		22.0*	0.2
GBD-34	32.98130	76.91970	Migmatitic gneiss	Deformed	N.D.		N.D.		N.D.		23.0*	0.2
GBD-36b	32.97470	76.91834	Pegmatite dike	Deformed	N.D.		N.D.		20.8	0.1	22.6*	0.1
GBD-38	32.96735	76.91959	Dike	Deformed	N.D.		N.D.		21.1	0.2	N.D.	
GBD-45b	32.90104	76.89998	Orthogneiss	Deformed	22.2	0.6	N.D.		N.D.		21.8	0.1
GBD- 51b	32.86728	76.83001	Orthogneiss	Deformed	37.0–33.2	0.8	N.D.		N.D.		25.9*	0.2
GBD-52b	32.86730	76.83075	Orthogneiss	Deformed	466.0	10.0	N.D.		21.4	0.1	25.1	0.2
Gianbul Valley												
GBD-57a	33.07651	77.15437	Schist	Deformed	N.D.		N.D.		20.2	0.2	20.4*	0.1
GBD-60b	33.07519	77.15351	Biotite schist	Deformed	N.D.		N.D.		21.4*	0.3	21.4	0.1
GBD- 63b	33.05773	77.11447	Pegmatite dike	Nondeformed	21.2	0.6	N.D.		19.7	0.1	19.8	0.1
GBD-64c	33.05815	77.11371	Granite dike	Nondeformed	N.D.		N.D.		19.8	0.2	19.6*	0.2
GBD- 64d	33.05815	77.11371	Orthogneiss	Deformed	37.6	0.7	N.D.		20.1	0.2	19.9	0.2
GBD-67a	33.05863	77.11839	Pegmatite dike	Deformed	N.D.		N.D.		19.9	0.2	N.D.	
GBD-79c	33.06576	77.13253	Biotite schist	Deformed	N.D.		N.D.		20.4	0.2	22.7	0.2
GBD-90b	33.05584	77.09758	Orthogneiss	Deformed	471.0	11.0	N.D.		20.2	0.2	21.6	0.2
GBD-100b	33.04867	77.03239	Biotite pegmatite	Deformed	N.D.		N.D.		21.1*	0.2	20.9*	0.2
GBD-101b	33.04776	77.02861	Migmatite	Deformed	22.8	0.7	N.D.		N.D.		22.5*	0.1

Sample no.	Lithology	Monazite†	95% conf.	Muscovite	±2σ
Z1§	Deformed dike	N.D.		22.0	0.1
Z2	Deformed dike	N.D.		20.9	0.1
Z3§	Leucogranite	N.D.		20.3	0.1
Z4	Leucogranite	N.D.		20.3	0.1
Z5§	Leucogranite	N.D.		19.6	0.1
Z6§	Leucogranite	N.D.		19.5	0.1
Z7§	Nondeformed dike	N.D.		19.7	0.1
Z8	Nondeformed dike	N.D.		19.6#	0.2
Z9§	Nondeformed dike	N.D.		19.4	0.1
Z10	Nondeformed dike	N.D.		19.3	0.1
V1–V5§	Leucogranite	22.2	0.2	N.D.	

Sample no.	Lithology	Monazite†	±2σ	Xenotime†	±2σ	Monazite**	95% conf.
02-10	Nondeformed dike	22.6	0.2	N.D.		N.D.	
02-13	Migmatite	N.D.		22.1	0.1	N.D.	
02-15§	Migmatite	N.D.		N.D.		22.6	0.9
02-16§	Migmatite	N.D.		N.D.		23.3	0.9
98-95	Migmatite	25.9	0.2	N.D.		26.6	0.2

Sample no.	Lithology	Monazite**	95% conf.
98-65	Nondeformed dike	23.0	1.5

Note: Ages for GBD- samples are from this study. Ages for Z and V samples are from Dèzes (1999) and Dèzes et al. (1999). Ages for 02- and 98- samples are from Robyr et al. (2006). N.D.—not determined.

*Preferred age.

†$^{207}Pb/^{235}U$ dates collected using thermal ionization mass spectrometry.

§Sampling location outside Gianbul and Miyar Valleys.

#Isochron age.

**Mean $^{208}Pb/^{232}Th$ ages.

a thermal ionization mass spectrometry (TIMS) $^{207}Pb/^{235}U$ date of 22.1 ± 0.1 Ma, and a monazite from a nearby migmatite (sample 98–95) has a TIMS $^{207}Pb/^{235}U$ date of 25.9 ± 0.2 Ma (Robyr et al., 2006) (Table 1); a single population of ion-microprobe $^{208}Pb/^{232}Th$ dates of ca. 26 Ma from the latter sample indicate that the TIMS date is an accurate age of monazite crystallization. At the base of the Khanjar shear zone, post-tectonic granite dikes have a TIMS date of 22.6 ± 0.2 Ma (sample 2–10; Robyr et al., 2006) and a mean laser ablation ICP-MS $^{232}Th/^{208}Pb$ date of 23.0 ± 1.5 Ma (for sample 98–65 excluding two analyses affected by common-Pb; Robyr et al., 2006), suggesting that ductile deformation, at least in the lower part of the shear zone, ceased by this time. Two other deformed metasedimentary migmatites in Miyar Valley (samples 2–15 and 2–16) gave ion-microprobe dates with a range of ~3 m.y. (Robyr et al., 2006), suggesting inheritance or prolonged recrystallization, so we interpret the youngest spot dates as the end of metamorphic (re)crystallization at ca. 22.5–22.0 Ma. Our new leucogranite dates are in accord with seven U-Pb TIMS monazite analyses from a deformed Cenozoic granite in the sillimanite zone of Gianbul Valley that yielded a range of $^{207}Pb/^{235}U$ dates from 29 to 22 Ma (Dèzes et al., 1999). The combined geochronology results indicate that waning stages of ductile shearing continued until ca. 22.1 Ma and had ceased by ca. 21 Ma.

Our thermochronology results from across the dome are consistent with muscovite $^{40}Ar/^{39}Ar$ dates for deformed granites (ca. 22–21 Ma) and nondeformed dikes (19.8–19.3 Ma) exposed in Gianbul Valley reported by Dèzes et al. (1999). Nondeformed dike $^{40}Ar/^{39}Ar$ dates are ~1 m.y. younger than nearby metamorphic sample dates; one explanation is that nondeformed dikes were emplaced after the country rocks cooled below muscovite Ar closure temperatures. However, $^{232}Th/^{208}Pb$ monazite dates for nondeformed dike sample 63 are ~2 m.y. older than coexisting muscovite $^{40}Ar/^{39}Ar$ dates, and a granite dike

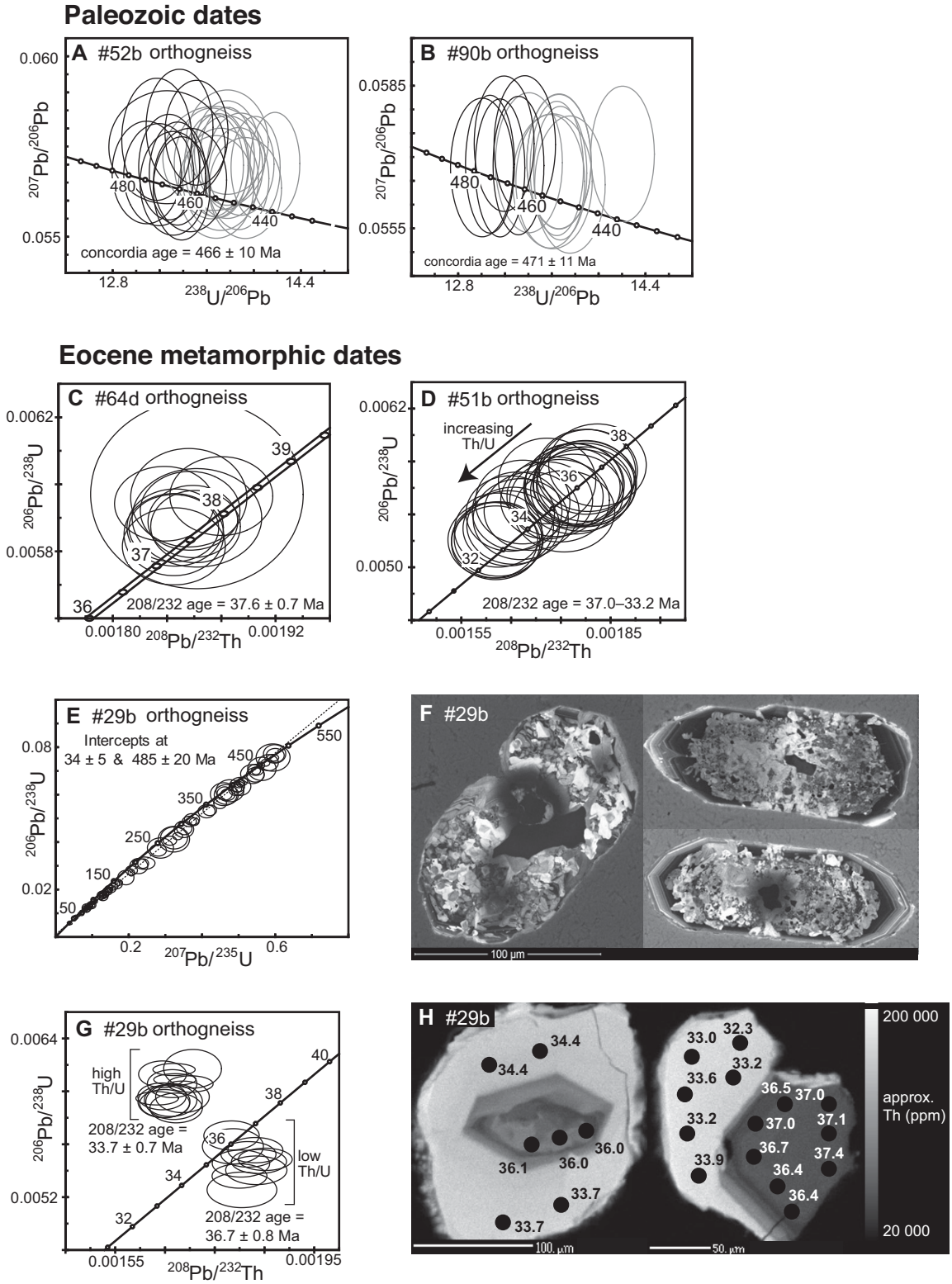

Figure 7 (*on this and following page*). U/Th-Pb geochronology concordia diagrams and relevant mineral textures. Paleozoic emplacement ages of the Kade orthogneiss are recorded for samples 52b (A) and 90b (B); black ellipses were used to calculate U-Pb concordia ages; discarded gray ellipses may have undergone Pb-loss or mixing with Cenozoic rims. Samples 64d (C), 51b (D), and 29b (G) have M1 metamorphic monazite dates from ca. 37 to 33 Ma. Cathodoluminescence images of inherited Paleozoic zircons in sample 29b (E and F) have annealing textures that suggest recrystallization during Cenozoic metamorphism. Electron microprobe images illustrate intragrain monazite textures for sample 29b (H), showing oscillatory zoning in metamorphic monazite indicative of crystallization in the presence of fluids.

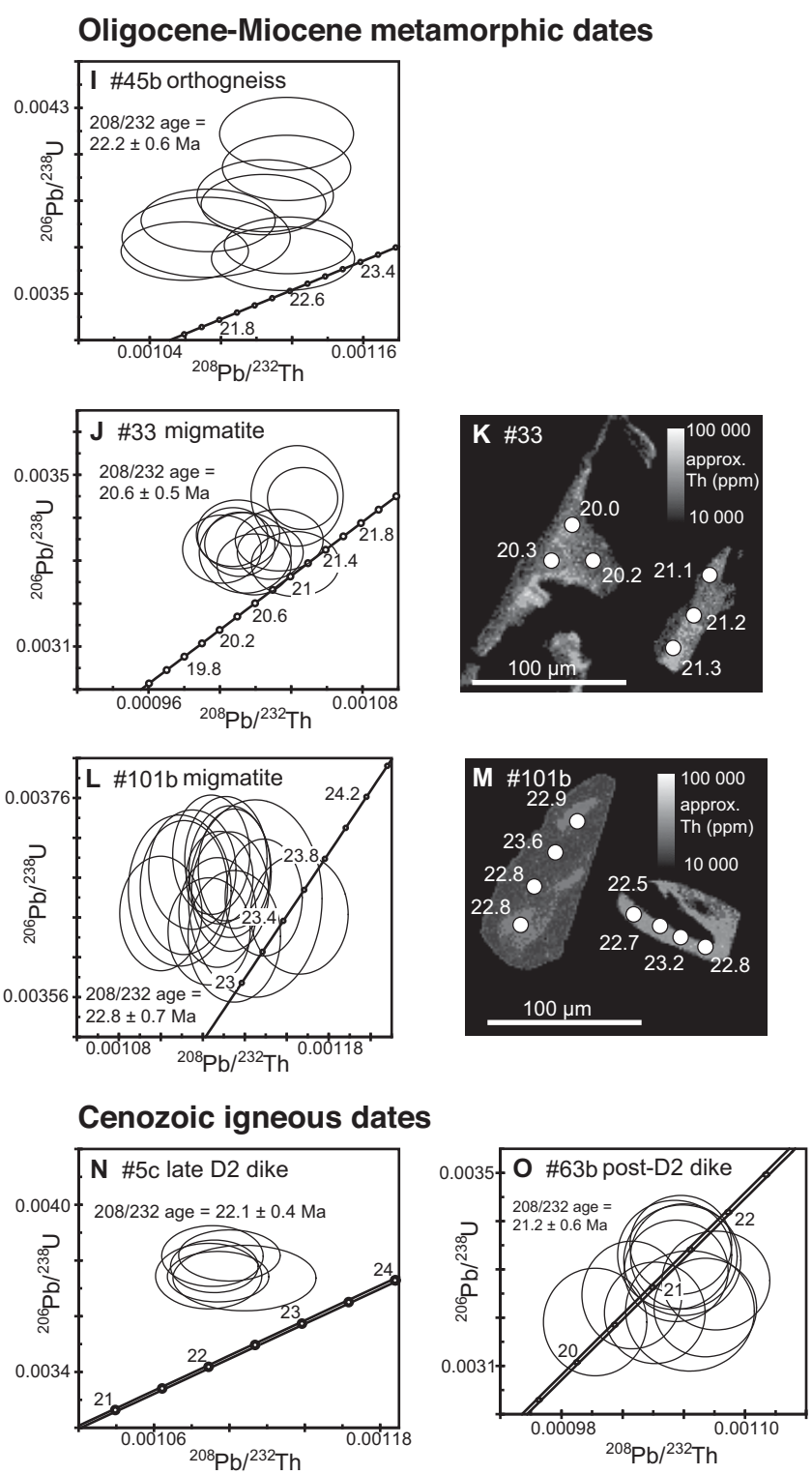

Figure 7 (*continued*). Monazite from samples 45b (I), 33 (J and K), and 101b (L and M) records late M2 metamorphism. Samples 5c (N) and 63b (O) (late- and post-tectonic leucogranite dikes, respectively) constrain the end of ductile deformation. For Cenozoic monazite, mean ^{232}Th-^{208}Pb dates and ±2σ error are reported.

intruded into country rock with temperatures <500 °C would cool in much less than 1 m.y. (e.g., Harris et al., 2000). If monazites in nondeformed dikes are inherited as xenocrysts or antecrysts (e.g., Lederer et al., 2013), ^{232}Th/^{208}Pb monazite dates may reflect protracted melting processes rather than dike emplacement. Different Ar closure temperatures for nondeformed dikes and country rock could also explain the younger ^{40}Ar/^{39}Ar muscovite dates observed for nondeformed dikes. Although 500 µm grains can undergo muscovite Ar closure at >50 °C higher than 100 µm grains (Harrison et al., 2009), finer muscovite grains were not observed in nondeformed samples. Other factors that affect Ar closure in muscovite—such as composition—may warrant further investigation.

Doming might be expected to bend isotherms upward and/or condense them in the core. The ^{40}Ar/^{39}Ar dates do not preserve such a trend. Instead, they decrease in age northward across the dome and are youngest on the northeast flank (Fig. 9A), which suggests that the observed ^{40}Ar/^{39}Ar trend is not due to doming. The simplest explanation is that isotherms had time to relax after doming ended and before Gianbul dome passed through muscovite Ar closure temperatures. The ^{40}Ar/^{39}Ar dates indicate that rocks in the Miyar Valley cooled below the muscovite Ar closure as early as ca. 21.4 Ma, ~1.2 m.y. before the northeast flank of the dome in Gianbul Valley. Making the first-order assumption that isotherms relaxed to near horizontal prior to cooling past the Ar muscovite closure, the inferred asymmetry is consistent with the exhumation of Gianbul dome as a southwest-tilted block in the footwall of the Zanskar normal fault after ca. 21.2 Ma. If so, the age gradient indicates that the footwall tilted 5°–10° after ca. 22 Ma as the Zanskar shear zone shallowed from between 25° to 30° to the present-day orientation of ~20° (Fig. 9C). Although ductile exhumation and magmatism ended by ca. 21.2 Ma, isotherms could have remained perturbed for at least several million years. Younger ^{40}Ar/^{39}Ar dates in the northeast could also be explained by the uniform exhumation of Gianbul dome before isotherms—perturbed by granite intrusions—fully relaxed. This might explain the discrepancy between monazite and muscovite dates for post-tectonic dike sample 63b, but it fails to account for the age discrepancy between adjacent metamorphic and post-tectonic dikes samples.

Late-stage ductile deformation within Gianbul dome was ongoing at ca. 22 Ma and ceased by 21 Ma, as demonstrated by deformed and nondeformed leucogranite crystallization ages. Furthermore, granites in Gianbul Valley cooled from hydrous granite solidus temperatures to

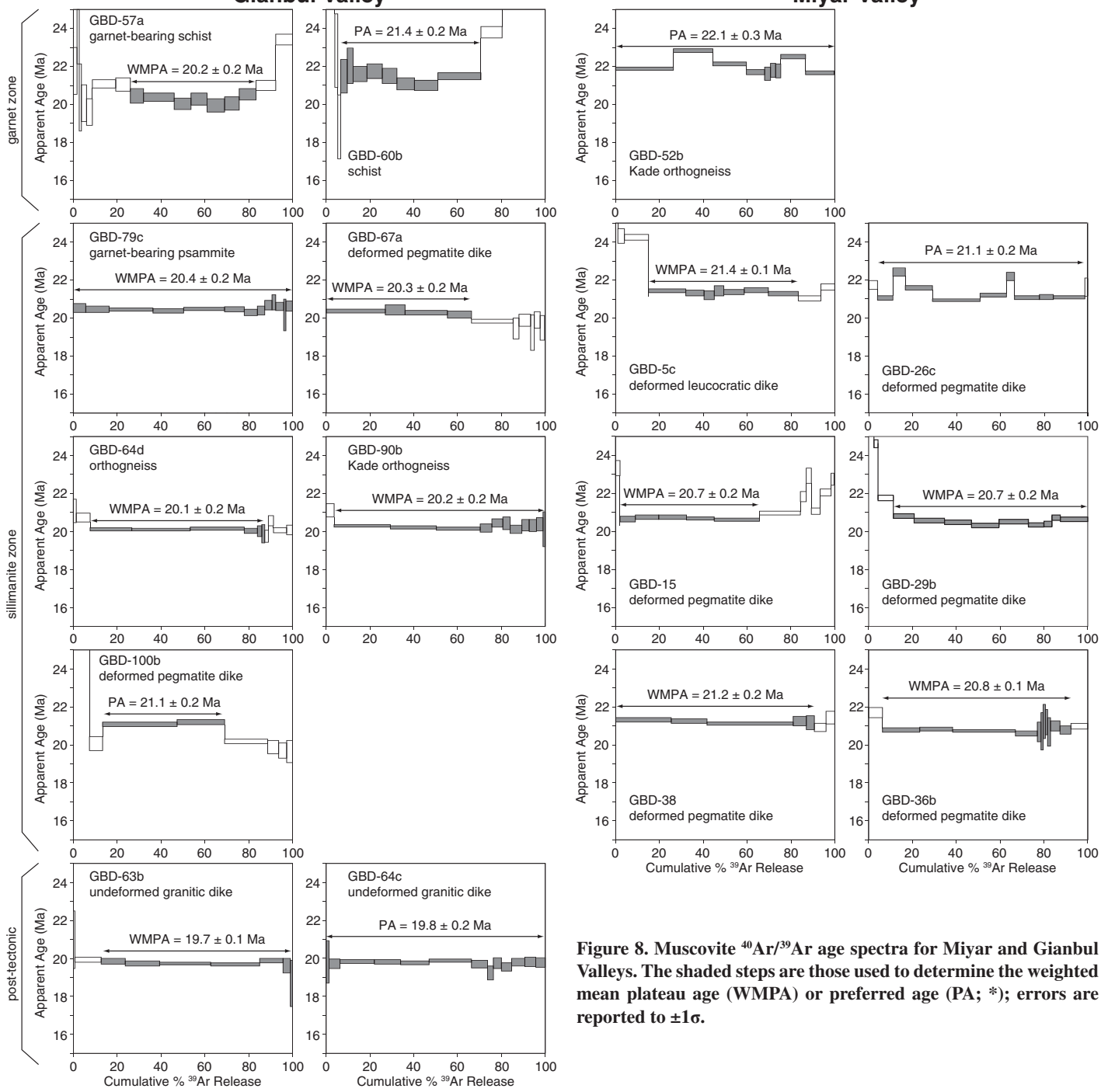

Figure 8. Muscovite $^{40}Ar/^{39}Ar$ age spectra for Miyar and Gianbul Valleys. The shaded steps are those used to determine the weighted mean plateau age (WMPA) or preferred age (PA; *); errors are reported to ±1σ.

muscovite Ar closure temperatures in less than 2 m.y. Nearby ^{87}Rb-^{86}Sr biotite dates of ca. 18.5 Ma for the Gumburanjun granite body (Ferrara et al., 1991) probably represent a lower-temperature closure at ~360 °C (e.g., Baxter et al., 2002) and indicate that cooling decelerated after muscovite Ar closure at 20 Ma in the Zanskar shear zone. Apatite fission-track and (U-Th)/He dates (closure temperature of <200 °C) reported by Deeken et al. (2011) increase systematically with elevation in Miyar Valley and exhibit no evidence of variable exhumation since 15 Ma. In contrast, apatite fission-track and (U-Th)/He dates from the footwall of the Zanskar normal fault indicate exhumation events at 14–10 and 9–6 Ma (Shurtleff et al., 2013); some of the inferred 5°–10° tilting in the footwall of the Zanskar normal fault likely occurred during these younger episodes of fault slip. The proposed fit of planar isotherms to the $^{40}Ar/^{39}Ar$ data may favor a >5 m.y. period of quiescence after doming and magmatism, allowing perturbed isotherms time to relax to near horizontal before tilting of the footwall block.

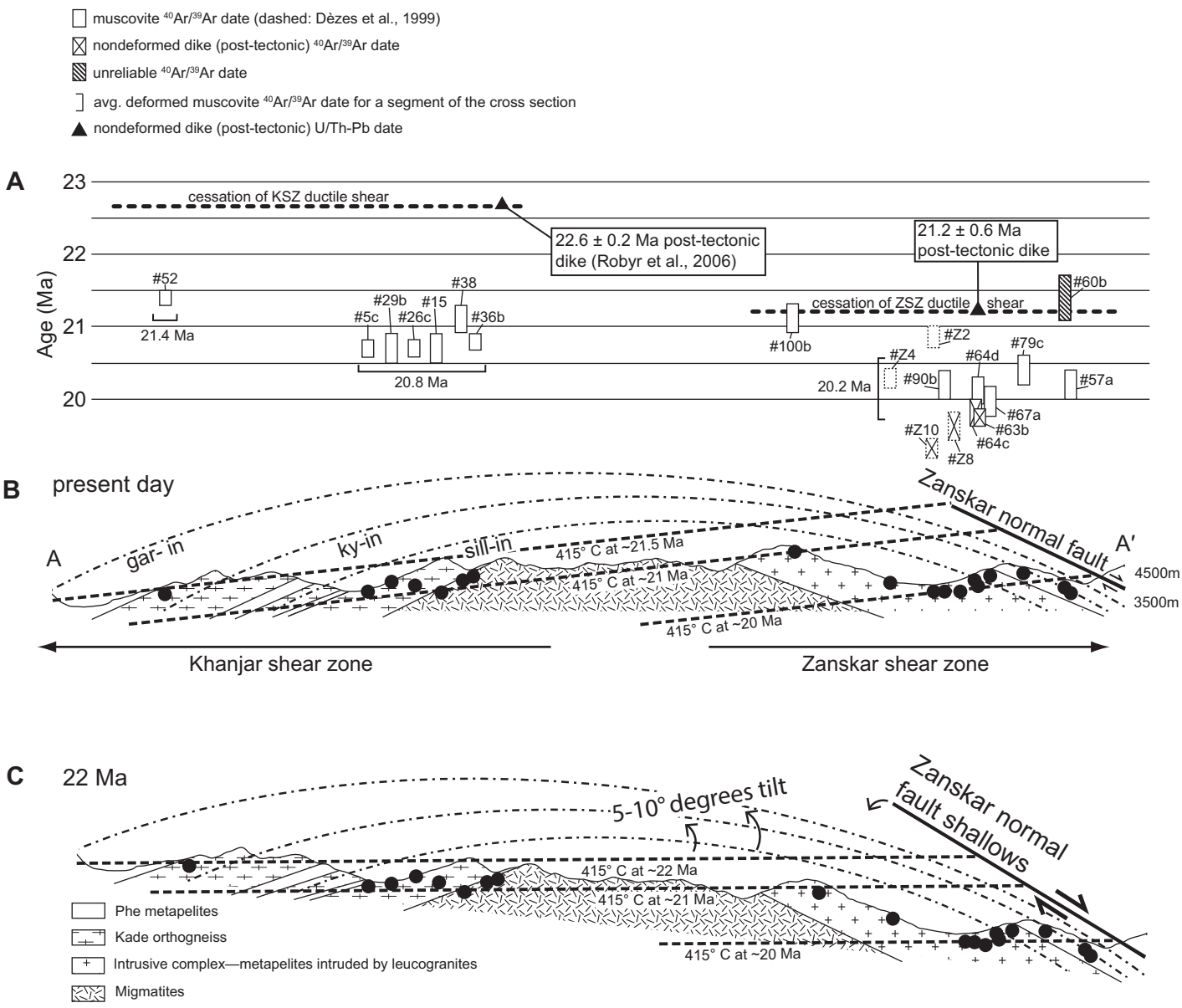

Figure 9. Summary of muscovite $^{40}Ar/^{39}Ar$ thermochronology across Gianbul dome showing exhumation in the footwall of the brittle Zanskar normal fault. (A) $^{40}Ar/^{39}Ar$ ages (rectangle heights represents 1σ uncertainties) along the Miyar–Gianbul Valley transect do not define a domal geometry. (B) Unlike domed metamorphic isograds, estimated ~415 °C chrontours (assumed to represent Ar muscovite closure) based on muscovite $^{40}Ar/^{39}Ar$ ages across the dome are tilted to the SW (gar—garnet, sill—sillimanite, ky—kyanite). (C) Assuming isotherms relaxed to horizontal prior to passing through muscovite Ar closure, reconstruction of a horizontal geotherm suggests that Gianbul was exhumed as a brittle block in the footwall of the Zanskar normal fault and tilted 5°–10° top-to-the-SW after ca. 22 Ma. ZSZ—Zanskar shear zone; KSZ—Khanjar shear zone.

DISCUSSION

Geochronologic Constraints on Ductile Deformation and Metamorphism

Prograde metamorphism is recorded by monazite (re)crystallization dates from 37 to 33 Ma across Gianbul dome and from 37 to 30 Ma near Gumburanjun (Walker et al., 1999); these ages likely represent the peak Barrovian M1 metamorphism caused by crustal thickening. Oscillatory zoning—commonly inferred to result from growth in the presence of melt—in M1 monazites may indicate that limited muscovite dehydration occurred in the Greater Himalayan Sequence during this phase. Northwest of Gianbul dome, where partial melting was less pervasive, Sm-Nd garnet dates from 33 to 28 Ma (Vance and Harris, 1999) record prograde burial-related metamorphism, and 27 Ma metamorphic monazite in upper Greater Himalayan Sequence metapelite (Horton and Leech, 2013) may reflect near-peak metamorphic conditions. Peak temperatures in the middle crust were likely attained by a combination of thermal re-equilibration, radiogenic heat production, and mechanical heating in shear zones. Retrograde

monazite growth at 26 Ma (Robyr et al., 2006) marks the transition from contractional M1 metamorphism and D1 deformation to extensional M2 metamorphism and D2 deformation. Based on U-Pb monazite ages from leucogranites that record contractional and extensional shear, Finch et al. (2014) also suggested that ca. 26 Ma marks the upper bound for the onset of ductile extension along the Zanskar shear zone.

The M1 Barrovian metamorphic isograds are telescoped within the Zanskar shear zone by D2 deformation, and they are overprinted in the core of Gianbul dome by M2 sillimanite-grade metamorphism and migmatization. As analogous structures, the Khanjar shear zone and Zanskar shear zone might be expected to have similar ages. However, the ages of discordant dikes demonstrate that ductile extension ended by 22.6 Ma in the Khanjar shear zone and 21.2 Ma within the Zanskar shear zone. If Miyar Valley exposes deeper portions of the Greater Himalaya Sequence, the age discrepancy suggests that shear zones within the Greater Himalayan Sequence propagated upward over time (Searle et al., 2007), or that distributed shear became condensed at the top of the sequence. Alternatively, longer-lived and/or higher strain within the Zanskar shear zone explains the greater degree to which isograds are collapsed within the Zanskar shear zone (Fig. 9). Continued exhumation after ca. 22 Ma was most likely accommodated by the overlying brittle Zanskar normal fault.

Timing of Gianbul Dome Formation

Gianbul dome probably did not form as a consequence of D1 contractional folding. Flexural flow folding within the crystalline nappe complex is a possible explanation for the proposed opposing-sense contractional deformation along limbs of the dome (e.g., Robyr et al., 2002, 2006, 2014) directed toward the fold hinge (top-to-the-NE in Miyar Valley and top-to-the-SW in Gianbul Valley). However, finite-element modeling conducted by Hudleston et al. (1996) suggests that flexural flow folding is unlikely in crystalline rock without high anisotropic competency, unless there are alternating low- and high-viscosity layers. Because the Kade orthogneiss preserves a contractional fabric but has neither a high anisotropic competency nor layers with alternating viscosity, flexural flow folding is an improbable mechanism for the domal morphology. The occurrence of distinct opposing-sense D1 contraction events is a more feasible explanation for opposing-sense D1 contractional structures.

Viewing the Zanskar shear zone and Khanjar shear zone as the same structure—which is compatible with both channel-flow and tectonic wedge models—raises the possibility that the top-to-the-NE kinematic indicators in the Khanjar shear zone are not D1 contractional structures (e.g., Robyr et al., 2002, 2006, 2014) but are instead early D2 structures coincident with early extension along the Zanskar shear zone. D1 top-to-the-SW structures have not been observed in the Khanjar shear zone, except possibly for one sample that has the top-to-the-NE C′ bands that crosscut top-to-the-SW C′ bands (Fig. 5C). Considering that D1 top-to-the-SW structures would have been reactivated or overprinted during D2 top-to-the-SW shearing, they may be difficult to identify. If the Khanjar shear zone and Zanskar shear zone were part of a bent roof fault (e.g., Yin, 2006), then the Khanjar shear zone segment may have been a back-thrust structure on the southern flank of the preexisting Gianbul dome. If, on the other hand, the Khanjar shear zone–Zanskar shear zone was originally a planar NE-dipping extensional shear zone, subsequent doming must have transposed the Khanjar shear zone segment into its current SW-dipping orientation. We favor the latter scenario for three reasons. First, the kinematic indicators are asymmetric across the dome: in the Khanjar shear zone, distributed top-to-the-NE shear is generally overprinted by top-to-the-SW shear in the upper levels, whereas the Zanskar shear zone exhibits almost exclusively top-to-the-NE shear that became concentrated in the upper levels. Second, whereas ductile shearing during passive roof faulting would have caused uniform flattening of footwall isograds, metamorphic isograds in Gianbul dome are more condensed within the Zanskar shear zone. Third, coeval opposing-sense ductile extension that ended at different times in the Khanjar shear zone and Zanskar shear zone suggests that the kinematic histories of the two faults diverged after doming.

Based on this rationale, we propose that doming postdated a transition from thrust to normal-sense motion in the upper Greater Himalayan Sequence (at ca. 26 Ma) and transposed early extensional features in the Khanjar shear zone. Ductile extension—and thus doming—ended prior to the emplacement of post-tectonic dikes at ca. 22.6–21.2 Ma. This is confirmed by the $^{40}Ar/^{39}Ar$ transect, which does not exhibit signs of doming after Gianbul dome cooled through Ar muscovite closure at ca. 22–21 Ma. Notably, the episode of ductile extension and associated doming in the middle crust from ca. 26 to 22 Ma coincides with syntectonic magmatism along the Karakoram shear zone (Valli et al., 2008), a ~1000 km strike-slip fault that has accommodated lateral extrusion in the western Himalaya. We suggest that this was a period of tectonic relaxation in response to weakening of thickened crust, during which lateral extrusion along crustal-scale strike-slip faults and southward extrusion of ductile middle crust simultaneously accommodated regionally extensive subsidence.

Doming Mechanisms

An adequate model for Gianbul dome formation must explain several key data sets: (1) core of anatectic melt, (2) synextensional leucogranites crosscutting gneisses, (3) ductile extensional deformation, (4) coeval opposing normal-sense shear zones, (5) asymmetric ductile extension, and (6) brittle normal slip along the previously ductile Zanskar shear zone (see Table 2 for comparison of doming models). Next, we discuss three principal factors—lithologic differences, upper-crustal extension, and decompression melting—that explain the formation of Gianbul dome.

Paleozoic Orthogneiss Megaboudins

With regard to gneiss dome formation, the nearly ubiquitous presence of Paleozoic orthogneiss in the cores of Himalayan gneiss domes is worth noting. In the northwest Himalaya, the Greater Himalayan Sequence consists of a NE-SW–trending series of domes cored by orthogneiss, including Barnaj, Bhazun, Cishoti, Chenab, Haptal, Umasi La, Poet La, and Gianbul domes (Herren, 1987; Kündig, 1989; Dèzes, 1999; Stephenson et al., 2001) (Fig. 2). In the eastern part of the orogen, orthogneiss is also documented in the cores of many North Himalayan gneiss domes, including Lhagoi Kangri (Watts and Harris, 2005), Mabja (Lee et al., 2004; Watts and Harris, 2005), Kampa (Quigley et al., 2006), and Kangmar (Lee et al., 2000) domes. Migmatitic textures in the Kade orthogneiss suggest that melting of orthogneiss and paragneiss generated Miocene magmas (Pognante et al., 1990; Pognante, 1992). Furthermore, bimodal $^{87}Sr/^{86}Sr$ ratios suggest that Miocene leucogranites in the western Himalaya had two source components: low initial $^{87}Sr/^{86}Sr$ (<0.76) from metawacke or metapelite and high $^{87}Sr/^{86}Sr$ (>0.76) from Paleozoic orthogneiss (Ferrara et al., 1991). The orthogneisses presumably formed during thin-skinned Paleozoic thrusting (Gehrels et al., 2003).

Field observations suggest that migmatization in Gianbul dome was most prevalent in paragneisses. Paleozoic orthogneiss protoliths probably contained less muscovite than surrounding metapelites, because existing muscovite formed during the retrogression of biotite and sillimanite (Pognante, 1992). Consequently, they would have produced less muscovite-dehydration melt and may have been more resistant to D2 deformation, undergoing less vertical thinning. If the Kade orthogneiss was more

TABLE 2. SUMMARY OF DOMING MODEL PREDICTIONS

Doming model	Structural and kinematic predictions	Chronologic predictions
1. Thrust duplexing during N-S contraction	Fault contact between core and cover Duplicate structural section Hanging wall originated at higher temperatures and greater depths than footwall Foliation may or may not be parallel to the fault Unidirectional lineations and reverse updip shear sense	Doming during contractional shear Doming during crustal thickening Asymmetric cooling with ages increasing updip
2. Tectonic wedge model (purely kinematic)	Top-to-the-SW shear overprinted by top-to-the-NE shear Parallel kinematic histories for both limbs of the dome	Both limbs record top-to-the-SW sense of shear Both limbs overprinted by top-to-the-NE sense of shear
3. Upper-crustal extension (i.e., core complex) (including instability in upper crust after plugged channel flow)	Doming in the footwall of a detachment fault Low-grade hanging wall above high-grade footwall Pure shear component Asymmetric simple shear (highest near hanging wall) Omitted structural/metamorphic section at fault Footwall strain increases toward the core-cover contact Unidirectional footwall lineations	Synchronous with localized upper-crustal extension Magmatism may occur throughout exhumation Coeval opposing normal-sense shear Asymmetric cooling with ages decreasing downdip
4. Diapirism in static stress field	Core of migmatite and/or leucogranite Concentric foliation Dome-up sense of shear Finite strain increases towards contact Syn- to postkinematic growth of metamorphic porphyroblasts in cover rocks Core-cover contact characterized by intrusion of core into cover Steep metamorphic field gradient in cover rocks	Simultaneous radial shearing Rapid ascent Rapid cooling Symmetrical cooling

competent than the surrounding metasedimentary rocks, it may have been a dome-scale megaboudin around which strain concentrated during vertical thinning. This could help explain the high-strain fabrics preserved in the uppermost Kade orthogneiss and overlying Phe metapelites (Figs. 4E and 4F). These observations suggest that strain and melt localization in the Greater Himalayan Sequence may have been related to the distribution of Paleozoic granites. However, vertical thinning around orthogneiss bodies neither accounts for decompression melting nor the magnitude of ductile shear accommodated by the Zanskar and Khanjar shear zones.

Upper-Crustal Extension

Our results indicate that the formation of Gianbul dome occurred between depths of ~40 km and 15 km during a period of extensional deformation and decompression melting in the upper Greater Himalayan Sequence that lasted from ca. 26 to 22 Ma (Fig. 10A). These constraints rule out doming mechanisms associated with D1 contraction, such as flexural folding and early thrust duplexing (Table 2). Also, our $^{40}Ar/^{39}Ar$ results suggest that Gianbul dome was exhumed as a coherent, rigid block in the footwall of the Zanskar normal fault (Fig. 9). Thus, upper-crustal exhumation-related processes since ca. 22 Ma cannot explain doming either.

We ascribe the SW-dipping, top-to-the-NE shear fabrics preserved in the Khanjar shear zone to the transposition of initially NE-dipping extensional deformation fabrics. Thus, doming occurred after considerable extensional offset had been accommodated by the Zanskar shear zone–Khanjar shear zone. Ductile exhumation (e.g., Lee et al., 2000; Beaumont et al., 2004; Jamieson et al., 2006) or thrusting (e.g., Yin, 2006) of the Greater Himalayan Sequence above a steepened segment of the footwall ramp could explain early domal morphology but fails to explain decompression melting. More likely, as shown in two-dimensional thermal-mechanical models by Rey et al. (2011), reactivation of the previously contractional Zanskar shear zone (Dèzes et al., 1999; Finch et al., 2014) and thinning of the upper crust created footwall pressure gradients that drove initial doming (Fig. 10B). This model accounts for near-isothermal decompression, asymmetric metamorphic isograds, and kinematics on either limb of Gianbul dome (Table 2).

A vertical pressure gradient below the thinning Tethyan Himalaya sequence may have initiated upward flow of Greater Himalayan Sequence crust that was sufficiently ductile (≥7% melt fraction; Rosenberg and Handy, 2005) but not yet highly buoyant. Destabilization of—and consequent extension in—upper crust above Gianbul dome could have been caused by southward channel tunneling of the Greater Himalayan Sequence and/or foreland-directed gravitational sliding of upper crust above ductile middle crust (e.g., Beaumont et al., 2004). Focused surface denudation along major rivers may also cause localized vertical pressure gradients in middle crust (e.g., Vannay et al., 2004; Montgomery and Stolar, 2006), but the fact that doming occurred during widespread orogen-perpendicular extension along the Zanskar shear zone suggests that doming was not driven by erosional processes. We conclude that Gianbul dome formation in the footwall of the Zanskar shear zone required upper-crustal extension; ductile flow driven by a vertical pressure gradient in the footwall of the Zanskar shear zone fits all of our observations, except the apparent links among decompression melting, ductile extension, and the cessation of doming.

Effects of Partial Melting

The high-Th monazite rims indicate that some silicate melt may have been present as early as 33 Ma (Fig. 7H), but there is no evidence that shear heating (which would have been severely moderated by partial melting) or advection of mantle heat via magmas (of which there are no signs) caused high percentages of melting. The near-isothermal decompression of Gianbul dome (Dèzes et al., 1999) and the resulting high-temperature–low-pressure metamorphism suggest that muscovite dehydration melting during decompression accounts for most of the melting observed in Gianbul Valley (Robyr et al., 2006). Because at least 10% of melt—and more likely ~30% melt—is required for positive buoyancy to drive doming (Teyssier and Whitney, 2002), sufficient melt for density-driven doming was probably not produced until decompression began.

Stockwork dikes, sills, and the voluminous Gumburanjun granite demonstrate that partial melt percentages were sufficient for ductile extrusion and eventually reached the 10%–40% necessary for a >0.2 g/cm^3 density contrast between leucocratic melt and garnet-biotite gneiss (Teyssier and Whitney, 2002). Thus, the

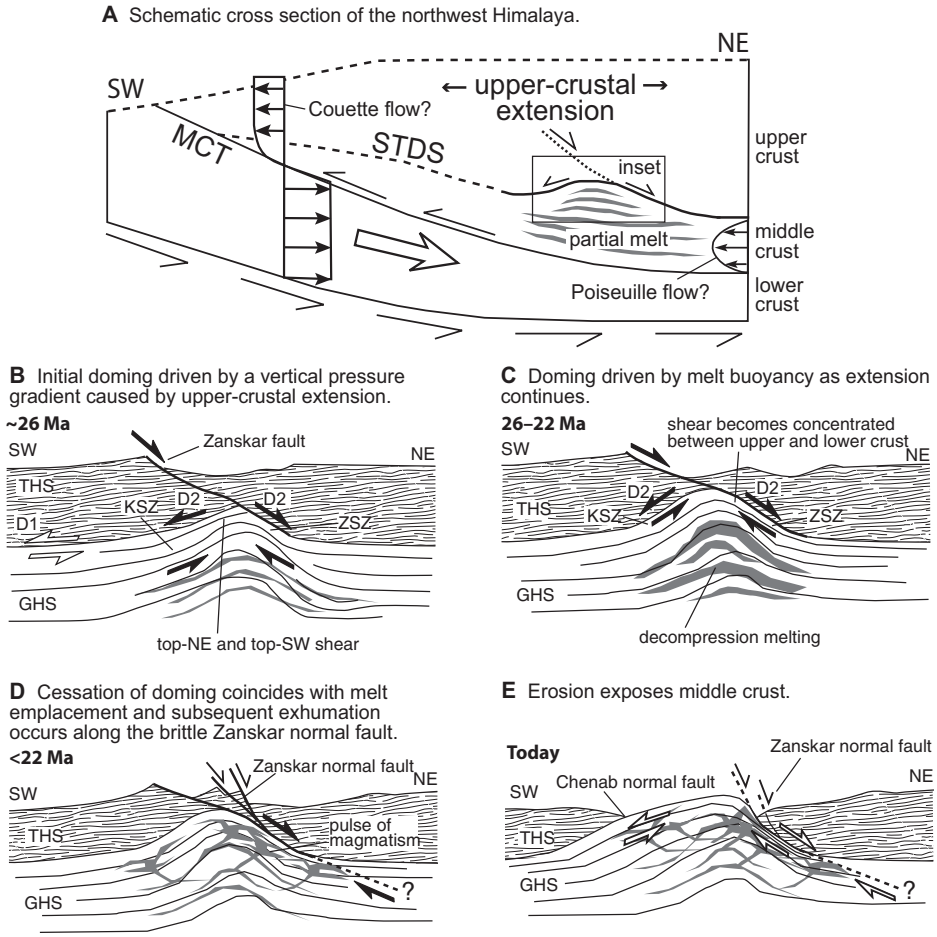

Figure 10. (A) Conceptual diagram (modified from Beaumont et al., 2004) showing the location of Gianbul dome formation in the middle crust. (B–E) Conceptual diagrams of Gianbul dome (see inset location in A) modified from Rey et al. (2011). Initial doming is driven by vertical pressure gradients below a thinning upper crust (B), after which decompression melting causes buoyancy-driven ascent of the dome (C). Melt emplacement marks the end of doming at ca. 22 Ma as normal-sense displacement in the Zanskar shear zone was transferred to the brittle Zanskar normal fault (D). Subsequent surface erosion has exposed the core of Gianbul dome at the surface (E). GHS—Greater Himalaya sequence; KSZ—Khanjar shear zone; MCT—Main Central thrust; STDS—South Tibetan detachment system; THS—Tethyan Himalaya sequence; ZSZ—Zanskar shear zone.

positive buoyancy of partial melts may have driven later stages of dome formation (e.g., Robyr et al., 2006). After exhumation began, and once sufficient melt was generated, a positive feedback among decompression, partial melting, and the positive buoyancy of partially melted rock (e.g., Teyssier and Whitney, 2002) could have driven doming (Fig. 10C). In this sense, Gianbul dome may be similar to other Himalayan gneiss domes, including Malashan dome (Aoya et al., 2005) and Renbu dome (Guo et al., 2008), which have also been attributed to diapiric rise of partially molten crust. Density-driven doming in a static stress field will yield a dome cored by plutons and/or migmatites with concentric foliation and radial and tangential stretching lineations (e.g., Schwerdtner et al., 1978; Brun and Pons, 1981; Dixon and Summers, 1983; Van Den Eeckhout et al., 1986; Jelsma et al., 1993) (Table 2). This set of geologic relationships is generally not observed in the northwestern Himalaya (Kündig, 1989; Vannay and Steck, 1995; Steck, 2003; Yin, 2006). In an extensional tectonic environment (e.g., Rey et al., 2011) or when crustal flow involves a lateral component (e.g., Whitney et al., 2004), buoyancy-driven doming can cause elongate domes with dominant unidirectional stretching lineations. Gianbul dome exhibits characteristics consistent with the latter scenarios: an elongate geometry, steeper-dipping, orogen-parallel limbs, a dominant orogen-perpendicular stretching lineation, and normal-sense shear.

Positive feedback between melting and exhumation best explains the existence of a single magmatic pulse at ca. 22 Ma, rather than a protracted period of generation and emplacement of leucogranites. The low viscosity and density of partially melted regions can only be sustained if the melt does not migrate. Furthermore, once emplaced in colder rock, leucogranite dikes and sills may crystallize rapidly (probably in less than 10 k.y. in the upper crust; Harris et al., 2000) and strengthen the host rock. The facts that leucogranites in Gianbul dome are exclusively late-D2 to post-tectonic and have a narrow age range from 22 to 21 Ma are consistent with accelerated doming immediately prior to a final pulse of magma migration (Fig. 10D). Leucogranite emplacement also coincided with the end of extensional shearing within the Khanjar shear zone at ca. 22.6 Ma, after which telescoping of the Barrovian metamorphic isograds continued within the Zanskar shear zone until ca. 21.2 Ma.

Implications for Tectonic Models

Because ductile extension within the Zanskar shear zone only lasted from ca. 26 to 21 Ma, midcrustal channel flow (e.g., Nelson et al., 1996; Beaumont et al., 2001; Grujic et al., 2002; Langille et al., 2010) would have been restricted to this relatively brief period of orogenesis in the northwestern Himalayan. Nevertheless, the predictions of the channel-flow model are useful for evaluating the orogen-scale forces that affected dome formation. According to the model, a low-viscosity layer in the middle crust (i.e., the Greater Himalayan Sequence) can begin tunneling if there is a horizontal gravitational potential energy gradient, but active channel-flow extrusion—driven by surface denudation—only commences once the channel penetrates the surface (Beaumont et al., 2004). Continued contraction after arrested channel tunneling, or plugged channel flow, could cause hinterland antiforms and crustal-scale folds. The presence of Tethyan sediments south of the Greater Himalayan Sequence (Thakur, 1998; Yin, 2006), the regional antiformal structure the Greater Himalayan Sequence, and the occurrence of gneiss domes are consistent with channel tunneling in the northwest Himalaya that was arrested prior to reaching the surface. A transient phase of southward Greater Himalayan Sequence tunneling could partially explain the development of domal structures in the northwest Himalaya. For Gianbul dome, however, the temporal link between the cessation of doming

and the pulse of granite emplacement suggests that doming was influenced by the positive buoyancy of high melt percentages. Instead of ductile exhumation of a channel below a passive hanging wall, thinning of the upper crust probably facilitated decompression melting, which gave way to buoyancy-driven ascent of middle crust.

The tectonic wedge model (Yin, 2006; Webb et al., 2007, 2013) provides an alternative explanation for the southward extrusion of the Greater Himalayan Sequence. This model suggests that, while the Greater Himalayan Sequence and overlying Tethyan Himalaya sequence were both thrust southward along the Main Central thrust, a change in the relative motion of the two thrust sheets caused a shift from top-to-the-N to top-to-the-S shear between them (in this case, along the Zanskar shear zone–Khanjar shear zone roof fault; Table 2). This explains the kinematics of deformation observed in the Zanskar shear zone, but it fails to explain (1) coeval opposing-sense extensional shear within the Zanskar shear zone and Khanjar shear zone; (2) top-to-the-NE shear overprinted by top-to-the-SW shear in the Khanjar shear zone; (3) the asymmetry of the condensed metamorphic isograds in Gianbul dome; and (4) the temporal and spatial links among penetrative D2 deformation, generation and emplacement of melts, and doming. Thus, neither the channel-flow model nor the tectonic wedging model independently explains the formation of Gianbul dome. However, localized vertical pressure gradients caused by upper-crustal extension coupled with melt buoyancy could explain Gianbul dome formation in the regional context of either model.

CONCLUSIONS

Gianbul dome exposes Greater Himalayan Sequence migmatite, Paleozoic orthogneiss, and metasedimentary rock crosscut by multiple generations of leucogranite dikes. These rocks expose a D2 penetrative deformation event characterized by a domed high-strain foliation and NE-SW–trending stretching lineation within the top-to-the-SW Khanjar shear zone on the southwest flank and the top-to-the-NE Zanskar shear zone on the northeast flank. Monazite U/Th-Pb geochronology and mica $^{40}Ar/^{39}Ar$ thermochronology across Gianbul dome record three distinct tectonometamorphic episodes: (1) Paleozoic intrusion of the Kade orthogneiss and associated granite dikes at ca. 470 Ma; (2) prograde M1 Barrovian metamorphism from 37 to 33 Ma during contractional D1 deformation; and (3) formation and exhumation of Gianbul dome between 26 and 22 Ma during high-temperature–low-pressure metamorphism, partial melting, and extensional D2 deformation. The late stages of the D2 ductile shearing persisted through 22 Ma, but subsequent exhumation was accommodated by ridged block tilting in the footwall of the Zanskar normal fault. Assuming isotherms relaxed to near horizontal prior to cooling through muscovite Ar closure, $^{40}Ar/^{39}Ar$ dates and low-temperature thermochronometry suggest that the footwall was tilted ~5°–10° top-to-the-SW after 22 Ma.

Our interpretation of Gianbul dome formation in the middle crust—driven first by upper-crustal extension and later by the positive buoyancy of partial melts—is neither entirely consistent with surface denudation–driven channel flow nor tectonic wedge propagation. We favor a model in which localized upper-crustal extension after ca. 26 Ma created vertical pressure gradients (e.g., Rey et al., 2011) in the upper Greater Himalayan Sequence and initiated upward flow of ductile crust. Our results are consistent with subsequent doming that was driven by positive feedbacks among dehydration melting, buoyancy, exhumation, and decompression. Doming culminated with the injection of anatectic melts into the upper levels of the dome at ca. 22 Ma, neutralizing the effects of melt buoyancy and potentially adding strength to the host rock as leucogranites crystallized. Despite these new constraints on dome formation, our inadequate understanding of the complex feedbacks among partial melting, buoyancy, and shearing—the forces driving rapid exhumation of middle crust—continues to inhibit the development of coherent models for gneiss doming in orogenic settings.

ACKNOWLEDGMENTS

The outstanding logistical planning provided by A. Bajaj and P. Chamoli and field assistance by R. Rana, T. Dorja, and M. Sing contributed to a successful field season. We thank An Yin and Rebecca Jamieson for thorough and constructive reviews, and Associate Editor Peter Cawood for his comments. Funding for this project was provided by National Science Foundation grants awarded to J. Lee (EAR-0838146) and to B. Hacker (EAR-0838264), and a National Science Foundation Graduate Research Fellowship awarded to F. Horton.

REFERENCES CITED

Aoya, M., Wallis, S.R., Terada, K., Lee, J., Kawakami, T., Wang, Y., and Heizler, M., 2005, North-south extension in the Tibetan crust triggered by granite emplacement: Geology, v. 33, no. 11, p. 853–856, doi:10.1130/G21806.1.

Baxter, E.F., DePaolo, D.J., and Renne, P.R., 2002, Spatially correlated anomalous $^{40}Ar/^{39}Ar$ "age" variations in biotites about a lithologic contact near Simplon Pass, Switzerland: A mechanistic explanation for excess Ar: Geochimica et Cosmochimica Acta, v. 66, p. 1067–1083, doi:10.1016/S0016-7037(01)00828-6.

Beaumont, C., Jamieson, R.A., Nguyen, M.H., and Lee, B., 2001, Himalayan tectonics explained by extrusion of a low-viscosity crustal channel coupled to focused surface denudation: Nature, v. 414, p. 738–742, doi:10.1038/414738a.

Beaumont, C., Jamieson, R.A., Nguyen, M.H., and Medvedev, S., 2004, Crustal channel flows: Numerical models with applications to the tectonics of the Himalayan-Tibetan orogen: Journal of Geophysical Research, v. 109, B06406, doi:10.1029/2003JB002809.

Brun, J.-P., and Pons, J., 1981, Strain patterns of pluton emplacement in a crust undergoing non-coaxial deformation, Sierra Morena, southern Spain: Journal of Structural Geology, v. 3, p. 219–229, doi:10.1016/0191-8141(81)90018-3.

Burg, J.P., Guiraud, M., Chen, G.M., and Li, G.C., 1984, Himalayan metamorphism and deformations in the North Himalayan Belt (southern Tibet, China): Earth and Planetary Science Letters, v. 69, no. 2, p. 391–400, doi:10.1016/0012-821X(84)90197-3.

Chen, Z., Liu, Y., Hodges, K.V., Burchfiel, B.C., Royden, L.H., and Deng, C., 1990, The Kangmar dome: A metamorphic core complex in southern Xizang (Tibet): Science, v. 250, no. 4987, p. 1552–1556, doi:10.1126/science.250.4987.1552.

Deeken, A., Thiede, R.C., Sobel, E.R., Hourigan, J.K., and Strecker, M.R., 2011, Exhumational variability within the Himalaya of northwest India: Earth and Planetary Science Letters, v. 305, no. 1, p. 103–114.

Dèzes, P.J., 1999, Tectonic and Metamorphic Evolution of the Central Himalayan Domain in Southeast Zanskar (Kashmir, India) [Ph.D. thesis]: Lausanne, Switzerland, University of Lausanne, 160 p.

Dèzes, P.J., Vannay, J.-C., Steck, A., and Bussy, F., 1999, Synorogenic extension: Quantitative constraints on the age and displacement of the Zanskar shear zone (northwest Himalaya): Geological Society of America Bulletin, v. 111, p. 364–374, doi:10.1130/0016-7606(1999)111<0364:SEQCOT>2.3.CO;2.

Dixon, J.M., and Summers, J.M., 1983, Patterns for total and incremental strain in subsiding troughs: Experimental centrifuged models of inter-diapir synclines: Canadian Journal of Earth Sciences, v. 20, p. 1843–1861, doi:10.1139/e83-175.

Epard, J.-L., and Steck, A., 2004, The eastern prolongation of the Zanskar shear zone (western Himalaya): Eclogae Geologicae Helvetiae, v. 97, no. 2, p. 193–212, doi:10.1007/s00015-004-1116-7.

Ferrara, G., Lombardo, B., Tonarini, S., and Turi, B., 1991, Sr, Nd and O isotopic characterization of the Gophu La and Gumburanjun leucogranites (High Himalaya): Schweizerische Mineralogische und Petrographische Mitteilungen, v. 71, p. 35–51.

Finch, M., Hasalova, P., Weinberg, R.F., and Fanning, C.M., 2014, Switch from thrusting to normal shearing in the Zanskar shear zone, NW Himalaya: Implications for channel flow: Geological Society of America Bulletin v. 126, p. 892–924, doi:10.1130/B30817.1.

Frank, W., Thöni, M., and Purtscheller, F., 1977, Geology and petrography of Kulu-South Lahul area: Colloq. Int. Cent. Natl. Rech. Sci., p. 147–172.

Gehrels, G.E., DeCelles, P.G., Martin, A., Ojha, T.P., Pinhassi, G., and Upreti, B.N., 2003, Initiation of the Himalayan orogen as an early Paleozoic thin-skinned thrust belt: GSA Today, v. 13, no. 9, p. 4–9, doi:10.1130/1052-5173(2003)13<4:IOTHOA>2.0.CO;2.

Grove, M., and Harrison, T., 1996, $^{40}Ar^*$ diffusion in Fe-rich biotite: The American Mineralogist, v. 81, no. 7–8, p. 940–951.

Grujic, D., Hollister, L.S., and Parrish, R.R., 2002, Himalayan metamorphic sequence as an orogenic channel: Insight from Bhutan: Earth and Planetary Science Letters, v. 198, no. 1, p. 177–191.

Guo, L., Zhang, J., and Zhang, B., 2008, Structures, kinematics, thermochronology and tectonic evolution of the Ramba gneiss dome in the northern Himalaya: Progress in Natural Science, v. 18, no. 7, p. 851–860, doi:10.1016/j.pnsc.2008.01.016.

Harris, N., Vance, D., and Ayres, M., 2000, From sediment to granite: Timescales of anatexis in the upper crust: Chemical Geology, v. 162, no. 2, p. 155–167, doi:10.1016/S0009-2541(99)00121-7.

Harrison, T.M., Lovera, O.M., and Grove, M., 1997, New insights into the origin of two contrasting Himalayan

granite belts: Geology, v. 25, no. 10, p. 899–902, doi:10.1130/0091-7613(1997)025<0899:NIITOO>2.3.CO;2.

Harrison, T.M., Célérier, J., Aikman, A.B., Hermann, J., and Heizler, M.T., 2009, Diffusion of ^{40}Ar in muscovite: Geochimica et Cosmochimica Acta, v. 73, no. 4, p. 1039–1051, doi:10.1016/j.gca.2008.09.038.

Hasalova, P., and Weinberg, R.F., 2011, Pure and simple shear partitioning at microscale revealed by quartz fabric in the South Tibetan detachment, Zanskar, NW India: Washington, DC, American Geophysical Union, Fall Meeting 2011, abstract T43C-2330.

Hauck, M.L., Nelson, K.D., Brown, L.D., Zhao, W., and Ross, A.R., 1998, Crustal structure of the Himalayan orogen at 90 east longitude from Project INDEPTH deep reflection profiles: Tectonics, v. 17, no. 4, p. 481–500, doi:10.1029/98TC01314.

Herren, E., 1987, The Zanskar shear zone: Northeast-southwest extension within the Higher Himalayas (Ladakh, India): Geology, v. 15, p. 409–413, doi:10.1130/0091-7613(1987)15<409:ZSZNEW>2.0.CO;2.

Hintersberger, E., Thiede, R.C., Strecker, M.R., and Hacker, B.R., 2010, East-west extension in the NW Indian Himalaya: Geological Society of America Bulletin, v. 122, no. 9–10, p. 1499–1515, doi:10.1130/B26589.1.

Honegger, K., Dietrich, V., Frank, W., Gansser, A., Thöni, M., and Trommsdorff, V., 1982, Magmatism and metamorphism in the Ladakh Himalayas (the Indus-Tsangpo suture zone): Earth and Planetary Science Letters, v. 60, p. 253–292, doi:10.1016/0012-821X(82)90007-3.

Horton, F., and Leech, M.L., 2013, Age and origin of granites in the Karakoram shear zone and Greater Himalaya Sequence, NW India: Lithosphere, v. 5, no. 3, p. 300–320, doi:10.1130/L213.1.

Hudleston, P.J., Treagus, S.H., and Lan, L., 1996, Flexural flow folding: Does it occur in nature?: Geology, v. 24, no. 3, p. 203–206, doi:10.1130/0091-7613(1996)024<0203:FFFDIO>2.3.CO;2.

Inger, S., 1998, Timing of an extensional detachment during convergent orogeny: New Rb-Sr geochronological data from the Zanskar shear zone, northwestern Himalaya: Geology, v. 26, p. 223–226, doi:10.1130/0091-7613(1998)026<0223:TOAEDD>2.3.CO;2.

Jamieson, R.A., Beaumont, C., Nguyen, M.H., and Grujic, D., 2006, Provenance of the Greater Himalayan Sequence and associated rocks: Predictions of channel flow models, *in* Law, R.D., Searle, M.P., and Godin, L., eds., Channel Flow, Ductile Extrusion, and Exhumation in Continental Collision Zones: Geological Society of London Special Publication 268, p. 165–182, doi:10.1144/GSL.SP.2006.268.01.07.

Jelsma, H.A., Van Der Beek, P.A., and Vinyu, M.L., 1993, Tectonic evolution of the Bindura–Shamva greenstone belt (northern Zimbabwe): Progressive deformation around diapiric batholiths: Journal of Structural Geology, v. 15, p. 163–176, doi:10.1016/0191-8141(93)90093-P.

Kirschner, D.L., Cosca, M.A., Masson, H., and Hunziker, J.C., 1996, Staircase ^{40}Ar/^{39}Ar spectra of fine-grained white mica: Timing and duration of deformation and empirical constraints on argon diffusion: Geology, v. 24, no. 8, p. 747–750, doi:10.1130/0091-7613(1996)024<0747:SAASOF>2.3.CO;2.

Kündig, R., 1989, Domal structures and high-grade metamorphism in the Higher Himalayan Crystalline, Zanskar Region, northwest Himalaya, India: Journal of Metamorphic Geology, v. 7, p. 43–55, doi:10.1111/j.1525-1314.1989.tb00574.x.

Langille, J., Lee, J., Hacker, B., and Seward, G., 2010, Middle crustal ductile deformation patterns in southern Tibet: Insights from vorticity studies in Mabja Dome: Journal of Structural Geology, v. 32, no. 1, p. 70–85, doi:10.1016/j.jsg.2009.08.009.

Law, R.D., Jessup, M.J., Searle, M.P., Francsis, M.K., Waters, D.J., and Cottle, J.M., 2011, Telescoping of isotherms beneath the South Tibetan detachment system, Mount Everest Massif: Journal of Structural Geology, v. 33, no. 11, p. 1569–1594, doi:10.1016/j.jsg.2011.09.004.

Lederer, G.W., Cottle, J.M., Jessup, M.J., Langille, J.M., and Ahmad, T., 2013, Timescales of partial melting in the Himalayan middle crust: Insight from the Leo Pargil dome, northwest India: Contributions to Mineralogy and Petrology, v. 166, p. 1415–1441.

Lee, J., Hacker, B.R., Dinklage, W.S., Wang, Y., Gans, P., Calvert, A., Wan, J., Chen, W., Blythe, A.E., and McClelland, W., 2000, Evolution of the Kangmar Dome, southern Tibet: Structural, petrologic, and thermochronologic constraints: Tectonics, v. 19, no. 5, p. 872–895, doi:10.1029/1999TC001147.

Lee, J., Hacker, B., and Wang, Y., 2004, Evolution of North Himalayan gneiss domes: Structural and metamorphic studies in Mabja Dome, southern Tibet: Journal of Structural Geology, v. 26, no. 12, p. 2297–2316, doi:10.1016/j.jsg.2004.02.013.

Lee, J., McClelland, W., Wang, Y., Blythe, A., and McWilliams, M., 2006, Oligocene-Miocene middle crustal flow in southern Tibet: geochronology of Mabja Dome: Geological Society of London, Special Publications, v. 268, no. 1, p. 445–469, doi:10.1144/GSL.SP.2006.268.01.21.

Le Fort, P., 1986, Metamorphism and magmatism during the Himalayan collision, *in* Coward, M.P., and Ries, A.C., eds., Collision Tectonics: Geological Society of London Special Publication 19, p. 159–172, doi:10.1144/GSL.SP.1986.019.01.08.

Le Fort, P., Cuney, M., Deniel, C., France-Lanord, C., Sheppard, S.M.F., Upreti, B.N., and Vidal, P.H., 1987, Crustal generation of the Himalayan leucogranites: Tectonophysics, v. 134, no. 1, p. 39–57, doi:10.1016/0040-1951(87)90248-4.

Makovsky, Y., Klemperer, S.L., Ratschbacher, L., and Alsdorf, D., 1999, Midcrustal reflector on INDEPTH wide-angle profiles: An ophiolitic slab beneath the India-Asia suture in southern Tibet?: Tectonics, v. 18, no. 5, p. 793–808, doi:10.1029/1999TC900022.

Mehta, P.K., 1977, Rb-Sr geochronology of the Kulu-Mandi belt: Its implications for the Himalayan tectogenesis: Geologische Rundschau, v. 66, p. 156–175, doi:10.1007/BF01989570.

Montgomery, D.R., and Stolar, D.B., 2006, Reconsidering Himalayan river anticlines: Geomorphology, v. 82, no. 1, p. 4–15.

Nelson, K.D., Zhao, W., Brown, L.D., Kuo, J., Che, J., Liu, X., Klemperer, S.L., Makovsky, Y., Meissner, R., and Mechie, J., 1996, Partially molten middle crust beneath southern Tibet: Synthesis of project INDEPTH results: Science, v. 274, no. 5293, p. 1684–1688, doi:10.1126/science.274.5293.1684.

Noble, S.R., and Searle, M.P., 1995, Age of crustal melting and leucogranite formation from U-Pb zircon and monazite dating in the western Himalaya, Zanskar, India: Geology, v. 23, p. 1135–1138, doi:10.1130/0091-7613(1995)023<1135:AOCMAL>2.3.CO;2.

Noble, S.R., Searle, M.P., and Walker, C.B., 2001, Age and tectonic significance of Permian granites in Western Zanskar, High Himalaya: The Journal of Geology, v. 109, p. 127–135, doi:10.1086/317966.

Pognante, U., 1992, Migmatites and leucogranites of Tertiary age from the High Himalayan Crystallines of Zanskar (NW India): A case history of anatexis of Palaeozoic orthogneisses: Mineralogy and Petrology, v. 46, p. 291–313, doi:10.1007/BF01173569.

Pognante, U., and Lombardo, B., 1989, Metamorphic evolution of the High Himalayan crystallines in SE Zanskar, India: Journal of Metamorphic Geology, v. 7, no. 1, p. 9–17, doi:10.1111/j.1525-1314.1989.tb00571.x.

Pognante, U., Castelli, D., Benna, P., Genovese, G., Oberli, F., Meier, M., and Tonarini, S., 1990, The crystalline units of the High Himalayas in the Lahul–Zanskar region (northwest India): Metamorphic–tectonic history and geochronology of the collided and imbricated Indian plate: Geological Magazine, v. 127, p. 101–116, doi:10.1017/S0016756800013807.

Quigley, M., Liangjun, Y., Xiaohan, L., Wilson, C.J., Sandiford, M., and Phillips, D., 2006, ^{40}Ar/^{39}Ar thermochronology of the Kampa Dome, southern Tibet: Implications for tectonic evolution of the North Himalayan gneiss domes: Tectonophysics, v. 421, no. 3, p. 269–297, doi:10.1016/j.tecto.2006.05.002.

Rey, P.F., Teyssier, C., Kruckenberg, S.C., and Whitney, D.L., 2011, Viscous collision in channel explains double domes in metamorphic core complexes: Geology, v. 39, no. 4, p. 387–390, doi:10.1130/G31587.1.

Robyr, M., Vannay, J.C., Epard, J.L., and Steck, A., 2002, Thrusting, extension, and doming during the polyphase tectonometamorphic evolution of the High Himalayan Crystalline Zone in NW India: Journal of Asian Earth Sciences, v. 21, p. 221–239, doi:10.1016/S1367-9120(02)00039-1.

Robyr, M., Hacker, B.R., and Mattinson, J.M., 2006, Doming in compressional orogenic settings: New geochronological constraints from the NW Himalaya: Tectonics, v. 25, TC2007, doi:10.1029/2004TC001774.

Robyr, M., Epard, J.-L., and El Korh, A., 2014, Structural, metamorphic and geochronological relations between the Zanskar shear zone and the Miyar shear zone (NW Indian Himalaya): Evidence for two distinct tectonic structures and implications for the evolution of the High Himalayan Crystalline of Zanskar: Journal of Asian Earth Sciences, v. 79, Part A, p. 1–15.

Rosenberg, C.L., and Handy, M.R., 2005, Experimental deformation of partially melted granite revisited: Implications for the continental crust: Journal of Metamorphic Geology, v. 23, p. 19–28, doi:10.1111/j.1525-1314.2005.00555.x.

Schwerdtner, W.M., Sutcliff, R.H., and Troeng, B., 1978, Patterns of total strain in the crustal region of immature diapirs: Canadian Journal of Earth Sciences, v. 15, p. 1437–1447, doi:10.1139/e78-150.

Searle, M.P., and Fryer, B.J., 1986, Garnet, tourmaline and muscovite-bearing leucogranites, gneisses and migmatites of the Higher Himalayas from Zanskar, Kulu, Lahoul and Kashmir, *in* Coward, M.P., and Ries, A.C., eds., Collision Tectonics: Geological Society of London Special Publication 19, p. 185–201, doi:10.1144/GSL.SP.1986.019.01.10.

Searle, M.P., and Rex, A.J., 1989, Thermal model for the Zanskar Himalaya: Journal of Metamorphic Geology, v. 7, p. 127–134, doi:10.1111/j.1525-1314.1989.tb00579.x.

Searle, M.P., Waters, D.J., Dransfield, M.W., Stephenson, B.J., Walker, C.B., Walker, J.D., and Rex, D.C., 1999, Thermal and mechanical models for the structural and metamorphic evolution of the Zanskar High Himalaya, *in* Mac Niocaill, C., and Ryan, P.D., eds., Continental Tectonics: Geological Society of London Special Publication 164, p. 139–156, doi:10.1144/GSL.SP.1999.164.01.08.

Searle, M.P., Simpson, R.L., Law, R.D., Parrish, R.R., and Waters, D.J., 2003, The structural geometry, metamorphic and magmatic evolution of the Everest Massif, High Himalaya of Nepal–South Tibet: Journal of the Geological Society of London, v. 160, no. 3, p. 345–366, doi:10.1144/0016-764902-126.

Searle, M.P., Stephenson, B., Walker, J., and Walker, C., 2007, Restoration of the Western Himalaya: Implications for metamorphic protoliths, thrust and normal faulting, and channel flow models: Episodes, v. 30, p. 242–257.

Shurtleff, B., Lee, J., Hager, C., Stockli, D., Van Vleck, D., and Blythe, A., 2013, Rapid middle to late Miocene slip along the Zanskar normal fault, Greater Himalayan Range, NW, India: Constraints from low-temperature thermochronometry: Geological Society of America Abstracts with Programs, v. 45, no. 7, p. 23.

Spring, L., Bussy, F., Vannay, J.C., Huon, S., and Cosca, M.A., 1993, Early Permian granitic dykes of alkaline affinity in the Indian High Himalaya of Upper Lahul and SE Zanskar: Geochemical characterization and geotectonic implications, *in* Treloar, P.J., and Searle, M.P., eds., Himalayan Tectonics: Geological Society of London Special Publication 74, p. 251–264, doi:10.1144/GSL.SP.1993.074.01.18.

Stahr, D.W., 2013, Kinematic Evolution, Metamorphism, and Exhumation of the Greater Himalayan Series, Sutlej River and Zanskar Regions of NW India [Ph.D. thesis]: Blacksburg, Virginia, Virginia Polytechnic Institute and State University, 115 p.

Stäubli, A., 1989, Polyphase metamorphism and the development of the Main Central thrust: Journal of Metamorphic Geology, v. 7, no. 1, p. 73–93, doi:10.1111/j.1525-1314.1989.tb00576.x.

Steck, A., 2003, Geology of the NW Indian Himalaya: Eclogae Geologicae Helvetiae, v. 96, p. 147–196.

Steck, A., Spring, L., Vannay, J.C., Masson, H., Stutz, E., Bucher, H., Marchant, R., and Tieche, J.C., 1993, Geological transect across the northwestern Himalaya in eastern Ladakh and Lahul (a model for the continental collision of India and Asia): Eclogae Geologicae Helvetiae, v. 86, no. 1, p. 219–263.

Stephenson, B.J., Searle, M.P., Waters, D.J., and Rex, D.C., 2001, Structure of the Main Central thrust zone and extrusion of the High Himalayan deep crustal wedge, Kishtwar-Zanskar Himalaya: Journal of the Geological Society of London, v. 158, p. 637–652, doi:10.1144/jgs.158.4.637.

Stutz, E., and Thöni, M., 1987, The Lower Paleozoic Nyimaling Granite in the Indian Himalaya (Ladakh): New Rb/Sr data versus zircon typology: Geologische Rundschau, v. 76, p. 307–315, doi:10.1007/BF01821076.

Teyssier, C., and Whitney, D.L., 2002, Gneiss domes and orogeny: Geology, v. 30, no. 12, p. 1139–1142, doi:10.1130/0091-7613(2002)030<1139:GDAO>2.0.CO;2.

Thakur, V.C., 1998, Structure of the Chamba nappe and position of the Main Central thrust in Kashmir Himalaya: Journal of Asian Earth Sciences, v. 16, p. 269–282, doi:10.1016/S0743-9547(98)00011-7.

Valli, F., Leloup, P.H., Paquette, J.-L., Arnaud, N., Li, H., Tapponnier, P., Lacassin, R., Guillot, S., Liu, D., and Deloule, E., 2008, New U-Th/Pb constraints on timing of shearing and long-term slip-rate on the Karakorum fault: Tectonics, v. 27, no. 5, TC5007, doi:10.1029/2007TC002184.

Vance, D., and Harris, N., 1999, Timing of prograde metamorphism in the Zanskar Himalaya: Geology, v. 27, p. 395–398, doi:10.1130/0091-7613(1999)027<0395:TOPMIT>2.3.CO;2.

Van Den Eeckhout, B., Grocott, B., and Vissers, R., 1986, On the role of diapirism in the segregation, ascent and final emplacement of granitoid magmas—Discussion: Tectonophysics, v. 127, p. 161–166, doi:10.1016/0040-1951(86)90086-7.

Vannay, J.-C., and Steck, A., 1995, Tectonic evolution of the High Himalaya in Upper Lahu (NW Himalaya, India): Tectonics, v. 14, p. 253–263, doi:10.1029/94TC02455.

Vannay, J.-C., Grasemann, B., Rahn, M., Frank, W., Carter, A., Baudraz, V., and Cosca, M., 2004, Miocene to Holocene exhumation of metamorphic crustal wedges in the NW Himalaya: Evidence for tectonic extrusion coupled to fluvial erosion: Tectonics, v. 23, no. 1, doi:10.1029/2002TC001429.

Walker, C.B., Searle, M.P., and Waters, D.J., 2001, An integrated tectonothermal model for the evolution of the High Himalaya in western Zanskar with constraints from thermobarometry and metamorphic modeling: Tectonics, v. 20, p. 810–833, doi:10.1029/2000TC001249.

Walker, J.D., Martin, M.W., Bowring, S.A., Searle, M.P., Waters, D.J., and Hodges, K.V., 1999, Metamorphism, melting, and extension: Age constraints from the High Himalayan slab of southeast Zanskar and northwest Lahaul: The Journal of Geology, v. 107, p. 473–495, doi:10.1086/314360.

Watts, D.R., and Harris, N.B., 2005, Mapping granite and gneiss in domes along the North Himalayan antiform with ASTER SWIR band ratios: Geological Society of America Bulletin, v. 117, no. 7–8, p. 879–886, doi:10.1130/B25592.1.

Webb, A.A.G., Yin, A., Harrison, T.M., Célérier, J., and Burgess, W.P., 2007, The leading edge of the Greater Himalayan Crystalline complex revealed in the NW Indian Himalaya: Implications for the evolution of the Himalayan orogen: Geology, v. 35, no. 10, p. 955–958, doi:10.1130/G23931A.1.

Webb, A.A.G., Yin, A., and Dubey, C.S., 2013, U-Pb zircon geochronology of major lithologic units in the eastern Himalaya: Implications for the origin and assembly of Himalayan rocks: Geological Society of America Bulletin, v. 125, no. 3–4, p. 499–522, doi:10.1130/B30626.1.

Whitney, D.L., Teyssier, C., and Vanderhaeghe, O., 2004, Gneiss domes and crustal flow, *in* Whitney, D.L., Teyssier, C., and Siddoway, C.S., eds., Gneiss Domes in Orogeny: Geological Society of America Special Paper 380, p. 15–33.

Yin, A., 2006, Cenozoic tectonic evolution of the Himalayan orogen as constrained by along-strike variation of structural geometry, exhumation history, and foreland sedimentation: Earth-Science Reviews, v. 76, no. 1, p. 1–131.

Science Editor: Nancy Riggs
Associate Editor: Peter A. Cawood

Manuscript Received 3 October 2013
Revised Manuscript Received 29 April 2014
Manuscript Accepted 3 May 2014

Printed in the USA